nature chemistry

ARTICLES

https://doi.org/10.1038/s41557-021-00641-1

Check for updates

A far-red hybrid voltage indicator enabled by bioorthogonal engineering of rhodopsin on live neurons

Shuzhang Liu[1,6], Chang Lin[1,6], Yongxian Xu[1,2,6], Huixin Luo[1], Luxin Peng[1], Xiangmei Zeng[1], Huangtao Zheng[1], Peng R. Chen[1,3] ✉ and Peng Zou[1,3,4,5] ✉

Membrane potential is a key aspect of cellular signalling and is dynamically regulated by an array of ion-selective pumps and channels. Fluorescent voltage indicators enable non-invasive optical recording of the cellular membrane potential with high spatial resolution. Here, we report a palette of bright and sensitive hybrid voltage indicators (HVIs) with fluorescence intensities sensitive to changes in membrane potential via electrochromic Förster resonance energy transfer. Enzyme-mediated site-specific incorporation of a probe, followed by an inverse-electron-demand Diels–Alder cycloaddition, was used to create enhanced voltage-sensing rhodopsins with hybrid dye–protein architectures. The most sensitive indicator, HVI-Cy3, displays high voltage sensitivity (−39% $\Delta F/F_0$ per 100 mV) and millisecond response kinetics, enabling optical recording of action potentials at a sampling rate of 400 Hz over 10 min across a large neuronal population. The far-red indicator HVI-Cy5 could be paired with optogenetic actuators and green/red-emitting fluorescent indicators, allowing an all-optical investigation of neuronal electrophysiology.

The membrane potential is a key biophysical signal that is central to life. The actions of ion-selective pumps and channels create a charge imbalance across the biological membrane, establishing a dynamic transmembrane electric field that can vary on the timescale of milliseconds. This electric field can, in turn, regulate the activities of an array of membrane-localized biomolecules, including voltage-gated ion channels and G-protein-coupled receptors[1]. The membrane potential has been traditionally measured with electrode-based techniques such as the whole-cell patch clamp approach. Despite their high sensitivity, electrode-based methods often suffer from a lack of spatial resolution, high invasiveness to cells and low throughput[2,3]. Optical recording of membrane potential offers an attractive alternative by avoiding the above limitations. Various voltage-sensitive fluorescent indicators have been developed to probe the membrane potential with high spatiotemporal resolution, high throughput and in a minimally invasive and highly parallel fashion. For example, genetically encoded voltage indicators (GEVIs) are used to report action potentials (APs) and subthreshold activities from genetically specified neuronal populations in cell cultures[4,5], brain slices[6,7] and living animals[2,3,8]. Because most of these GEVIs are based on green or red fluorescent proteins (FPs), their fluorescence emission has been limited to wavelengths below 650 nm.

A bright and sensitive far-red indicator is highly desired because it could facilitate the simultaneous recording of membrane voltage and other important physiological signals, such as calcium dynamics and neurotransmitter release[9]. In addition, a redshifted excitation spectrum could enable crosstalk-free pairing of the imaging probe with optogenetic actuators such as ion-selective channels and pumps, many of which are activated by blue and yellow light, thus allowing an all-optical investigation of neural circuit electrophysiology[10,11]. Among the rare examples of far-red voltage sensors, rhodopsin-based GEVIs (QuasArs[10,12], Archers[13] and Archon[14]) sense membrane potential via electrochromism and could emit at >650 nm (Table 1). However, the native fluorescence of rhodopsin is approximately two orders of magnitude weaker than a bright organic dye because of the low fluorescence quantum yield of its retinal chromophore[15]. Thus, applications of these rhodopsin-based GEVIs often require intense excitation light (>80 W cm^{-2})[10,14], raising concerns about an excessive heating effect and phototoxicity[16]. Near-infrared voltage-sensing dyes have been developed to achieve voltage imaging in cell cultures and brain slices (Table 1)[17–20]. Although photo-activation and enzymatic uncaging approaches have enabled the cell-specific labelling of voltage-sensing dyes, they have not been extended to far-red indicators[21–23]. Recently, a chemigenetic voltage indicator called Voltron was engineered by fusing a self-labelling protein tag, HaloTag, to a voltage-sensing microbial rhodopsin, Ace2 from *Acetabularia acetabulum*[24]. Voltron$_{635}$ has an emission peak at 656 nm and reports APs in cultured neurons with a modest sensitivity of approximately −3.5% fluorescence change over baseline level ($\Delta F/F_0$) per AP (Table 1)[24].

In this Article, we report a novel approach to achieving voltage imaging in the far-red spectrum with high speed and sensitivity. We employ enzyme-mediated probe incorporation to site-specifically conjugate a *trans*-cyclooctene moiety to an Ace2 mutant, which is subsequently derivatized with tetrazine-conjugated organic fluorophores via the inverse-electron-demand Diels–Alder cycloaddition (IEDDA) reaction. The resulting hybrid voltage indicators

[1]College of Chemistry and Molecular Engineering, Synthetic and Functional Biomolecules Center, Beijing National Laboratory for Molecular Sciences, Key Laboratory of Bioorganic Chemistry and Molecular Engineering of the Ministry of Education, Peking University, Beijing, China. [2]School of Life Sciences, Tsinghua University, Beijing, China. [3]Peking-Tsinghua Center for Life Sciences, Beijing, China. [4]PKU-IDG/McGovern Institute for Brain Research, Beijing, China. [5]Chinese Institute for Brain Research (CIBR), Beijing, China. [6]These authors contributed equally: Shuzhang Liu, Chang Lin, Yongxian Xu. ✉e-mail: pengchen@pku.edu.cn; zoupeng@pku.edu.cn

Table 1 | Summary of existing far-red voltage indicators

Name	Type	Sensitivity ($\Delta F/F_0$)		Illumination intensity (W cm^{-2})	Emission peak (nm)	Ref.
		% per 100 mV[a]	% per AP[b]			
QuasAr2	GEVI	90	48	300–800	715	Ref. [10]
Archer1	GEVI	85	40	88	>660	Ref. [13]
Archon1	GEVI	81	30	~80	>660	Ref. [14]
Di-2-ANEP(F)PTEA	Dye	NA	12.4	NA	632	Ref. [20]
Indocyanine green	Dye	−1.9	NA	0.5	>800	Ref. [19]
BeRST 1	Dye	24	9.5	20	683	Ref. [17]
Voltron$_{635}$	Hybrid	−4	−3.5	0.5–2	656	Ref. [24]
HVI-Cy5	Hybrid	−19.6	−12.8	0.2–1.2	662	This study

[a]Depolarization from −70 mV to 30 mV. [b]Measured in cultured hippocampal neurons. NA, not available.

(HVIs) feature a dye–protein architecture that exhibits a strong electrochromic effect, in which the dye fluorescence intensities are dynamically modulated by the strength and direction of the transmembrane electric field. The most sensitive indicator, HVI-Cy3, displays a voltage sensitivity of −39% $\Delta F/F_0$ per 100 mV and millisecond response kinetics. Voltage imaging with HVI-Cy3 in cultured human embryonic kidney 293 T (HEK293T) cells revealed gap junction-mediated electrical coupling. The most far-redshifted indicator, HVI-Cy5, reports neuronal APs with a sensitivity 3.6-fold higher than Voltron$_{635}$ (−12.8% versus −3.5% $\Delta F/F_0$, Table 1) and is spectrally orthogonal to green/red-emitting sensors, which is beneficial for multiplexed fluorescence imaging of neuronal activities. We further demonstrate the power of simultaneous voltage sensing and voltage control by combining HVI-Cy5 with blueshifted optogenetic actuators to achieve an all-optical investigation of electrophysiology in cultured neurons.

Results

Construction of hybrid voltage indicators. To obtain a far-red-sensing HVI, we first performed bioorthogonal and site-specific fluorophore labelling of rhodopsin on live neurons. With our strategy, fluorophore labelling takes place via two steps: enzyme-mediated probe incorporation and bioorthogonal conjugation (Fig. 1a and Extended Data Fig. 1). In the first step, a functional handle (for example, azide or *trans*-cyclooctene) is introduced to the extracellular side of the Ace2 rhodopsin via the PRIME ('probe incorporation mediated by enzyme') technique using an engineered bacterial lipoic acid ligase (LplA) on live cells[25–27]. Briefly, the carboxyl group in the substrate is activated by adenosine triphosphate (ATP) into an adenylate intermediate, before being ligated to the amine group on the lysine side chain of a 13-amino-acid short peptide called LAP (Fig. 1a). Before we started, we considered the choice of LAP fusion site in Ace2 rhodopsin. In previous PRIME applications, LAP has been fused to either the N or C terminus of protein targets to avoid affecting protein folding and to facilitate enzyme recognition[25–27]. In the specific case of Ace2, however, C-terminal fusion is not possible because it is located at the intracellular side and is thus inaccessible to the enzyme. N-terminal fusion is also problematic because this may interfere with the N-terminal signal sequence that is crucial for the proper membrane trafficking of Ace2. Our solution is to insert LAP into the first extracellular loop of Ace2 (Fig. 1a). In addition, introducing fluorophore at this loop enhances the Förster resonance energy transfer (FRET) efficiency of the hybrid sensor, presumably due to a shorter donor–acceptor distance compared to N-terminal fusion[28].

In the second step, the functional handle is subsequently derivatized with an organic fluorophore through a bioorthogonal chemical reaction. In the resulting dye–protein architecture, because of the spectral overlap and the short distance between the fluorophore donor and the rhodopsin's retinal chromophore acceptor, the reporter fluorescence is partially quenched via the FRET mechanism, the efficiency of which depends on the membrane potential through an electrochromic effect[2,15]. We compared several bioorthogonal reactions on neuronal cell membrane (Extended Data Fig. 1). First, copper-assisted alkyne-azide cycloaddition (CuAAC) was ruled out because of its strong neural toxicity induced by the presence of copper at micromolar concentrations[28]. We then evaluated strain-promoted alkyne-azide cycloaddition (SPAAC). Although this copper-free click reaction allowed cell-specific labelling in live neurons, we observed a high fluorescence background (Extended Data Fig. 1 and Supplementary Table 1), presumably due to the high hydrophobicity of the dibenzocyclooctyne (DBCO)-conjugated fluorophore[29]. The IEDDA reaction between *trans*-cyclooctene (TCO) and tetrazine (Tz) is attractive because of its high biocompatibility and fast reaction kinetics ($k \approx 10^3$–10^6 M^{-1} s^{-1})[27,29–33]. Given that this reaction has recently been repurposed as a bioorthogonal cleavage reaction with certain TCO–Tz pairs[34–38], we carefully considered the choice of TCO structure. The position of carbamate substitution group on the TCO ring is critical, because derivatives such as 2-TCO may undergo further rearrangement and elimination after the initial cycloaddition with Tz[34–38]. We thus started with **4-TCO** and commercially available Tz-conjugated dyes as the IEDDA pair and optimized the probe concentration and labelling time (Extended Data Fig. 1). We further verified that the reaction caused negligible background staining (Extended Data Fig. 1 and Supplementary Table 1) and little perturbation to neuronal electrophysiology and cell viability (Supplementary Fig. 1).

We also sought to improve the voltage sensitivity through site-directed mutagenesis of Ace2. Based on the crystal structure (Fig. 1) and previous biophysical studies, the proton acceptor Asp81 residue (homologous to Asp95 and Asp85 in archaerhodopsin-3 and bacterial rhodopsin, respectively[39]) is involved in the acid–base equilibrium of the Schiff base in the retinal binding pocket, which critically influences the rhodopsin absorption spectrum and the voltage-sensing process[40,41]. We thus focused on the Asp81 site and screened nine mutants. Among these, we identified ^{Asp81Cys}Ace2 as the best-performing rhodopsin protein scaffold in terms of sensitivity, signal-to-noise ratio (SNR; Fig. 1c and Supplementary Table 2) and membrane trafficking (Extended Data Fig. 2) in cultured rat hippocampal neurons. Importantly, this single mutation also abolished the steady-state photocurrent of the wild-type Ace2, which is a highly desirable property for voltage indicators (Extended Data Fig. 2). Taken together, we have optimized the conjugation chemistry

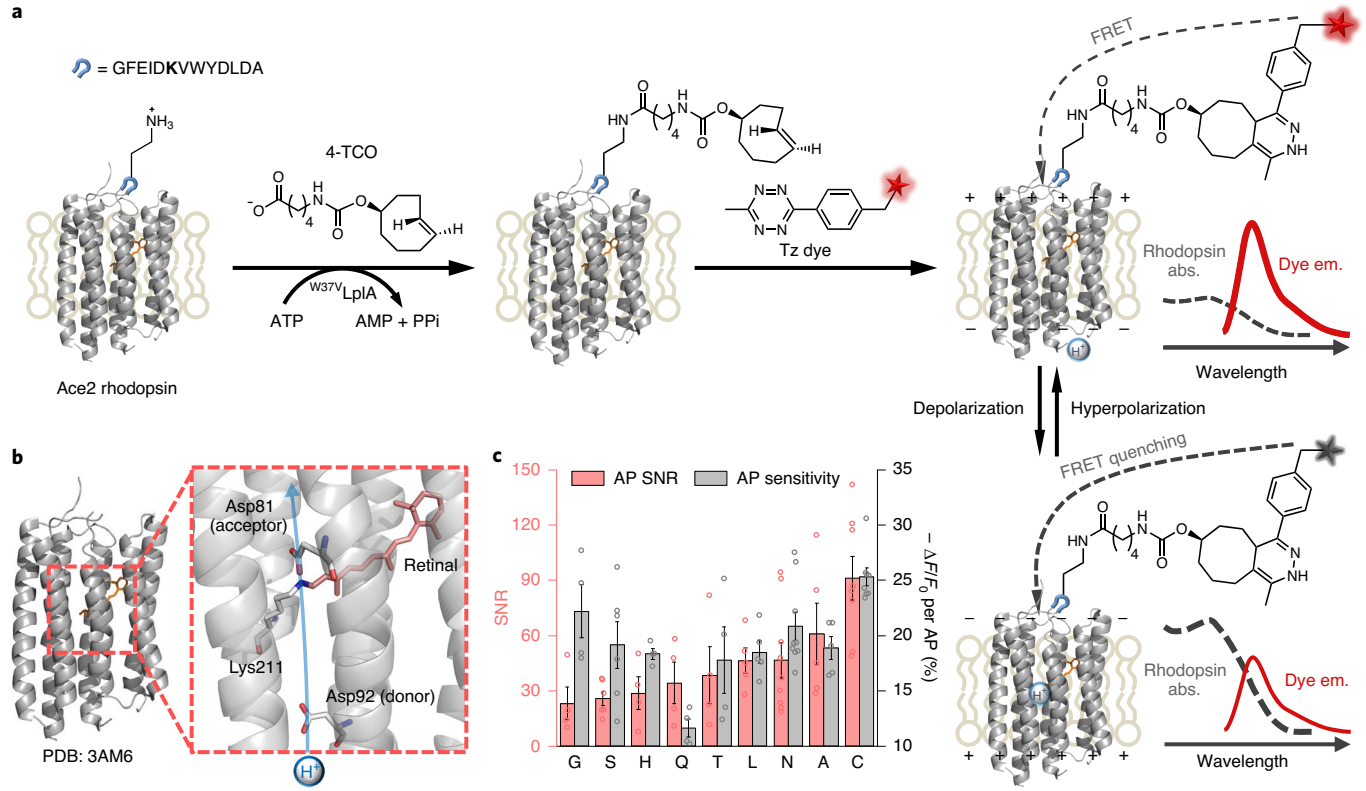

Fig. 1 | Design of HVIs through bioorthogonal and site-specific engineering of rhodopsin on the neuronal cell membrane. a, Scheme of fluorescence labelling. In the first step, the LplA ligase mutant installs a bioorthogonal functional handle (**4-TCO**) onto the central lysine residue in the peptide substrate (LAP). ATP is consumed to generate the adenylate intermediate at the active site, which subsequently reacts with the amine to form an amide linkage. In the second step, the fluorophore is conjugated via an inverse-electron-demand Diels–Alder reaction. Voltage sensing occurs via the electrochromic FRET (eFRET) mechanism. Upon membrane depolarization, the FRET quenching efficiency increases, leading to lower fluorescence emission from the donor. **b**, Crystal structure of light-sensitive proton pump Ace2. A zoomed-in view of the retinal binding pocket is shown on the right. Proton translocates from Asp92 to Asp81 via the Schiff base linkage between Lys211 and the retinal chromophore (PDB: 3AM6). **c**, Voltage sensitivities and the AP detection signal-to-noise ratios (SNRs) of Ace(D81X) mutants. Rat hippocampal neurons expressing Ace(D81X) were labelled with Tz-Cy3. Stimulated AP firing was triggered via current injection using a whole-cell patch clamp method. $n = 4$ cells (D81G), 6 cells (D81S), 4 cells (D81H), 4 cells (D81Q), 4 cells (D81T), 5 cells (D81L), 9 cells (D81N), 5 cells (D81A) and 8 cells (D81C), respectively. Error bars represent s.e.m.

(IEDDA) and obtained an enhanced rhodopsin protein scaffold (^{Asp81Cys}Ace2), which we used for all subsequent experiments.

Cellular characterization of HVI series. We created a panel of ^{Asp81Cys}Ace2–fluorophore hybrid voltage indicators (hereafter referred to as HVIs) through the IEDDA reaction with commercially available tetrazine–fluorophore conjugates (Supplementary Table 8). Notably, to construct our far-red HVI we used Cy5 as the fluorophore because of its desired excitation/emission spectrum (ex. peak at 649 nm; em. peak at 670 nm) and high molecular brightness (extinction coefficient $\varepsilon = 2.5 \times 10^5\,M^{-1}\,cm^{-1}$, fluorescence quantum yield $\Phi = 27\%$)[42]. We chose 3-methyl-6-Cy5-substituted Tz (mTz-Cy5), which is a more stable molecule than Tz-Cy5 during chemical synthesis and has a high reactivity towards **4-TCO**. More importantly, the introduction of a methyl group at the 3-position would substantially stabilize the tetrazine ring towards amines and thiols that are highly abundant in the cellular milieu[27,33].

We characterized the dynamic ranges and response kinetics of HVIs in HEK293T cells (Fig. 2a and Supplementary Fig. 2). The membrane potential was controlled via whole-cell voltage clamp and varied linearly between −100 mV and 100 mV. Fluorescence image series were acquired simultaneously, and whole-cell-averaged fluorescence from a manually selected region of interest was used for quantitation. For comparison, two FP-based GEVIs—Ace2N-mNeon[2] and VARNAM[3]—were included in the analysis. Among these, HVI-Cy3 showed the highest sensitivity ($\Delta F/F_0 = -39.1 \pm 0.8\%$ per 100 mV; mean ± s.e.m.) and millisecond response kinetics (half-life $\tau_{1/2} = 1.70 \pm 0.07$ ms in the depolarizing step (mean ± s.e.m.); Fig. 2b,c and Supplementary Table 3). Even the most redshifted indicator—HVI-Cy5—exhibited a remarkable sensitivity ($\Delta F/F_0 = -19.6 \pm 0.8\%$ per 100 mV; Fig. 2b,c and Supplementary Table 3). Consistent with the model of electrochromic FRET, voltage sensitivities of HVIs are dependent on the dye emission spectra (Fig. 2d).

To demonstrate the high voltage sensitivity and fast response of HVI-Cy3, we applied this probe to visualize electrical coupling in cultured HEK293T cells. At the contact sites between neighbouring cells, hexameric connexin proteins on the plasma membrane assemble into gap junction channels that allow the intercellular exchange of molecules smaller than ~1,000 Da (refs. [43,44]). Because ions can also diffuse across the gap junction, a monolayer of cultured HEK293T cells can be electrically connected across a long distance. Traditionally, electrical coupling has been investigated using a dual patch clamp technique, which is technically challenging. For voltage imaging, we labelled cells with HVI-Cy3 and controlled the membrane potential of a single cell via patch clamp, while simultaneously monitoring the fluorescence from the entire field of view of dozens of cells (Extended Data Fig. 3). The fluorescence response to the command voltage decayed exponentially as a function of distance between the measured cell and the patch pipette, with a

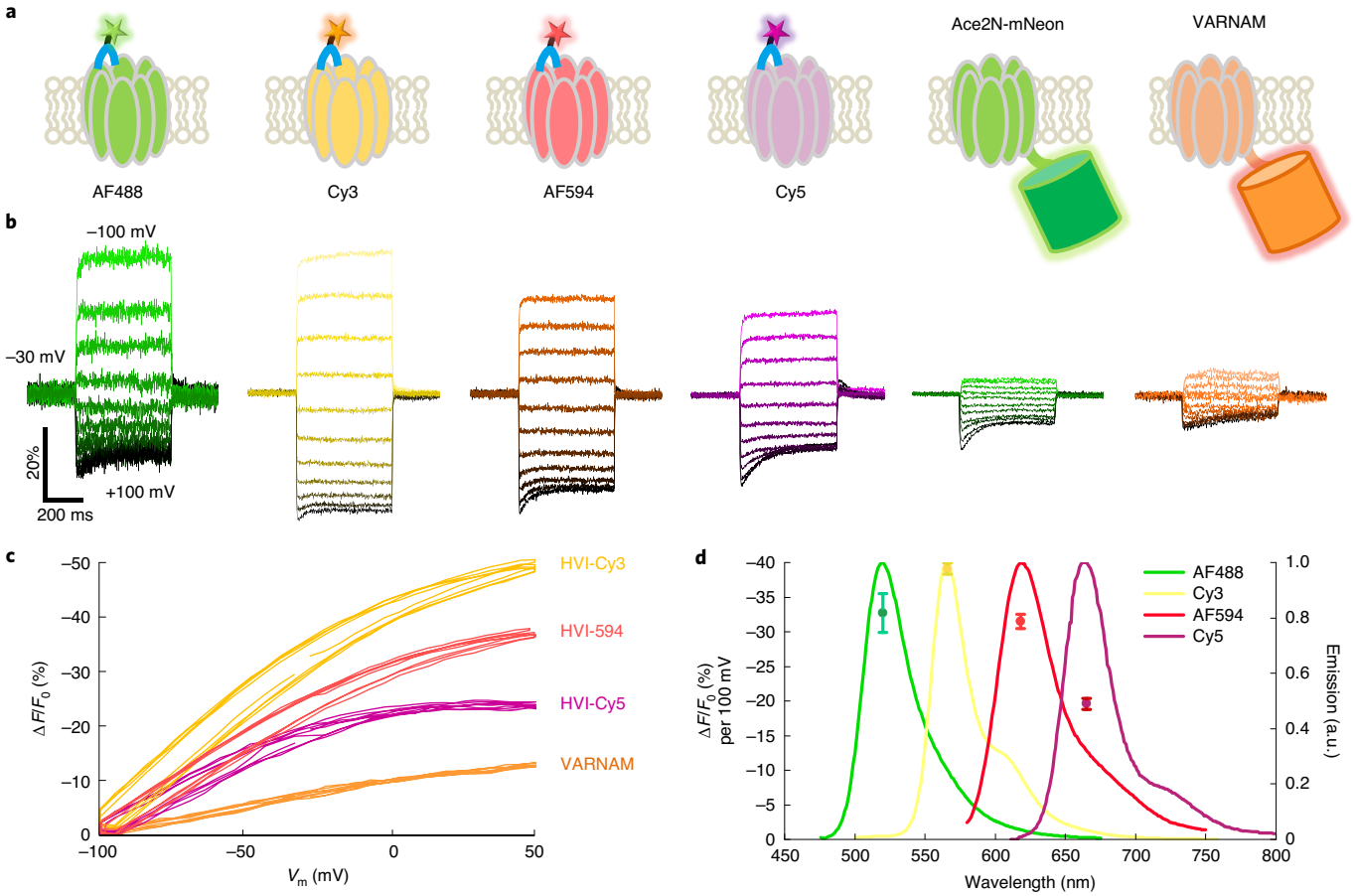

Fig. 2 | Characterization of the HVI voltage response dynamic range and kinetics in HEK293T cells. a, Scheme of HVIs labelled with AF488/Cy3/AF594/Cy5, Ace2N-mNeon and VARNAM. **b**, Comparison of voltage sensitivities of HVIs and GEVIs in HEK293T cells. The membrane potential was controlled via whole-cell voltage clamp, and a series of step waveforms were applied from ***−100 mV to 100 mV in increments of 20 mV. The image sampling rates were 1,058 Hz and 484 Hz for HVIs and GEVIs, respectively. The sensitivity has been normalized to the fluorescence at membrane voltage*** $V_m = -30$ mV. **c**, Fluorescence–voltage (*F*–*V*) curves of HVIs and VARNAM. The membrane potentials of the HEK293T cells were controlled by whole-cell voltage clamp. A triangle waveform from −100 mV to +50 mV was applied for four cycles with a period of 6 s, and the fluorescence signal was recorded simultaneously at a camera frame rate of 10 Hz. **d**, An overlay of the dynamic range ($\Delta F/F_0$, where F_0 is the fluorescence at −70 mV) and emission spectra of the HVI series. $n = 5$ cells (HVI-488), 9 cells (HVI-Cy3), 7 cells (HVI-594) and 7 cells (HVI-Cy5). Error bars represent s.e.m.

length constant of ~100 µm. In addition, the fluorescence response between electrically coupled cells appeared synchronized at the temporal resolution of 5 ms (Extended Data Fig. 3).

In cultured rat hippocampal neurons, the high dynamic range of the HVI series has led to the sensitive detection of membrane voltage dynamics. For example, HVI-Cy3 and HVI-Cy5 faithfully report AP spikes with sensitivities of $\Delta F/F_0 = -25.3 \pm 0.8\%$ and $-12.8 \pm 0.9\%$ per AP, respectively, which compare favourably with the FP-based GEVIs Ace2N-mNeon ($-4.9 \pm 0.3\%$) and VARNAM ($-5.3 \pm 0.3\%$) (Fig. 3a,b, Extended Data Fig. 4 and Supplementary Table 3). Notably, the most redshifted indicator—HVI-Cy5—is 3.6-fold more sensitive than the spectrally similar Voltron$_{635}$ (−12.8% versus −3.5% $\Delta F/F_0$ per AP; Table 1 and Supplementary Table 4)[24]. In addition, HVI-Cy3 could respond to small changes in subthreshold potential with SNR = 9.8 ± 1.1 per 8 mV of depolarization at a camera frame rate of 484 Hz under laser illumination of 4.9 W cm^{-2} (Fig. 3c, Supplementary Fig. 3 and Supplementary Table 5). Taking advantage of the higher photostability of HVI-Cy3 (photobleaching half-life $t_{1/2} = 430 \pm 64$ s) relative to FP-based GEVIs (Ace2N-mNeon $t_{1/2} = 87 \pm 4$ s; VARNAM $t_{1/2} = 154 \pm 7$ s; Extended Data Fig. 4 and Supplementary Table 6), we achieved continuous voltage imaging at 500 Hz over 10 min. Our data show spontaneous AP firing as well as subthreshold activities, and the SNR remained high after 10 min of light illumination (Fig. 3d). Across a field of view of 452 µm by 161 µm, our method revealed synchronized activities of cultured rat hippocampal neurons (Extended Data Fig. 5).

We evaluated the potential phototoxicity of HVIs through patch clamp electrophysiology and a CellTiter-Glo assay, which measures cellular ATP concentrations. In all cases, the neurons were 100% viable after light illumination, as they robustly fired APs when stimulated by current injection ($n = 18$ cells). Furthermore, no significant changes in neuronal electrophysiology or cell viability were observed in cultured neurons expressing HVI-Cy5 after 5 min of illumination with a 637 nm laser at 0.5 W cm^{-2} (Supplementary Figs. 4 and 5). For HVI-Cy3, 10 min of illumination with a 532 nm laser at 1 W cm^{-2} caused no significant changes in membrane capacitance, resting potential, rheobase or AP amplitude and width. However, we did observe a reduction in membrane resistance (377 ± 42 MΩ versus 738 ± 91 MΩ, $P = 0.0065$; Supplementary Fig. 4), indicating that care must be taken to reduce the laser power for long-term voltage imaging with HVI-Cy3.

Multiplexed voltage imaging with HVI-Cy5. The far-red emission spectrum of HVI-Cy5 allowed us to simultaneously monitor the membrane potential and other physiological signals such as Ca^{2+} (Fig. 4a,b), intracellular pH (Extended Data Fig. 6) and extracel-

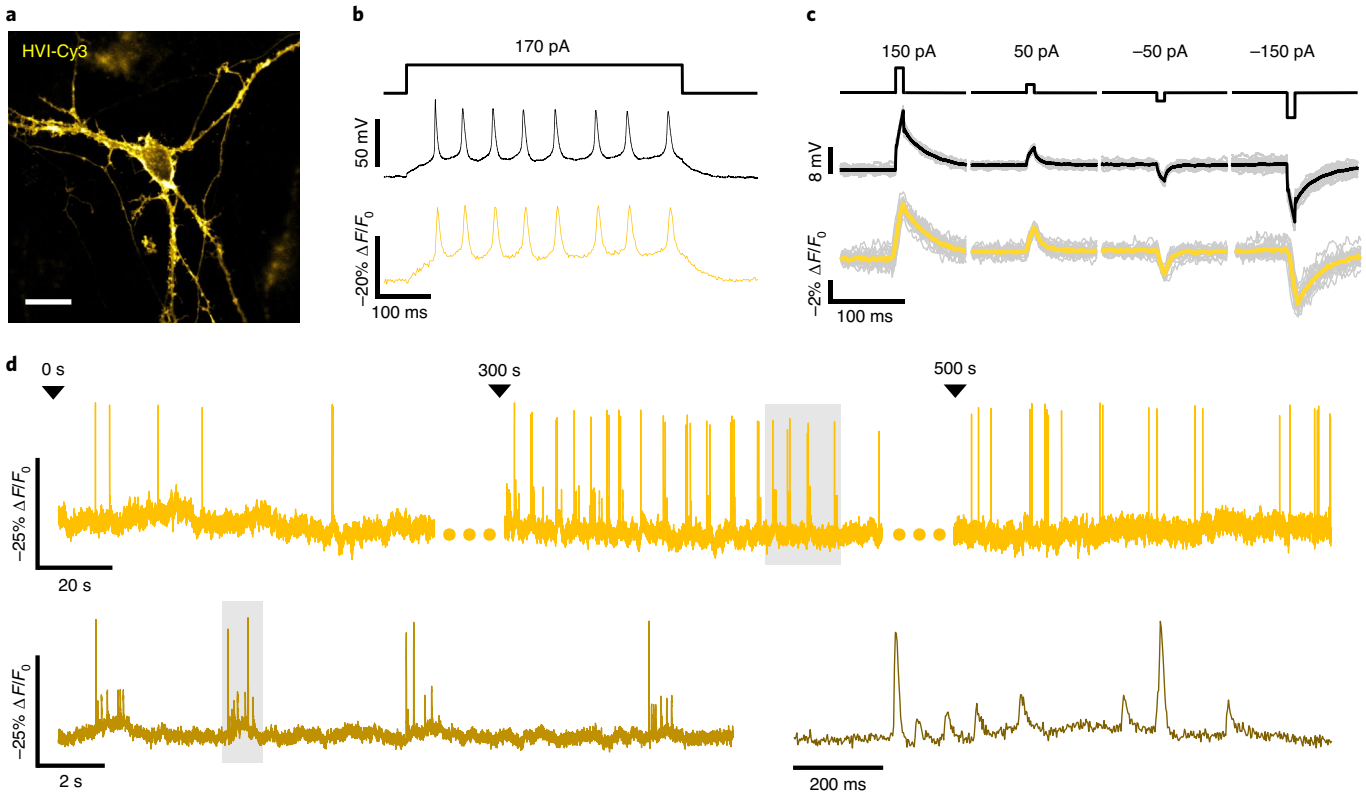

Fig. 3 | Voltage imaging with HVIs in cultured rat hippocampal neurons. a, Representative confocal images of a rat hippocampal neuron expressing HVI-Cy3. Scale bar, 20 μm. **b**, Simultaneous electrical recording (black trace) and HVI-Cy3 imaging (orange trace, sampling rate of 484 Hz) of an AP spike train from a neuron stimulated by injection of a current of 170 pA for 500 ms. **c**, Simultaneous electrical recording (black trace) and HVI-Cy3 imaging (orange trace, sampling rate of 484 Hz) of the subthreshold voltage activities of neurons stimulated by 10-ms weak current injections. Twenty successive stimuli (grey) are superimposed, and the averaged trace of HVI-Cy3 fluorescence is shown in orange. **d**, Voltage imaging of a single neuron with HVI-Cy3 at 500 Hz for 10 min under illumination of ~1 W cm^{-2}. The fluorescence signals for 0–100 s, 300–400 s and 500–600 s are shown as orange traces. Two successive zoomed-in views of the shaded regions are shown at the bottom.

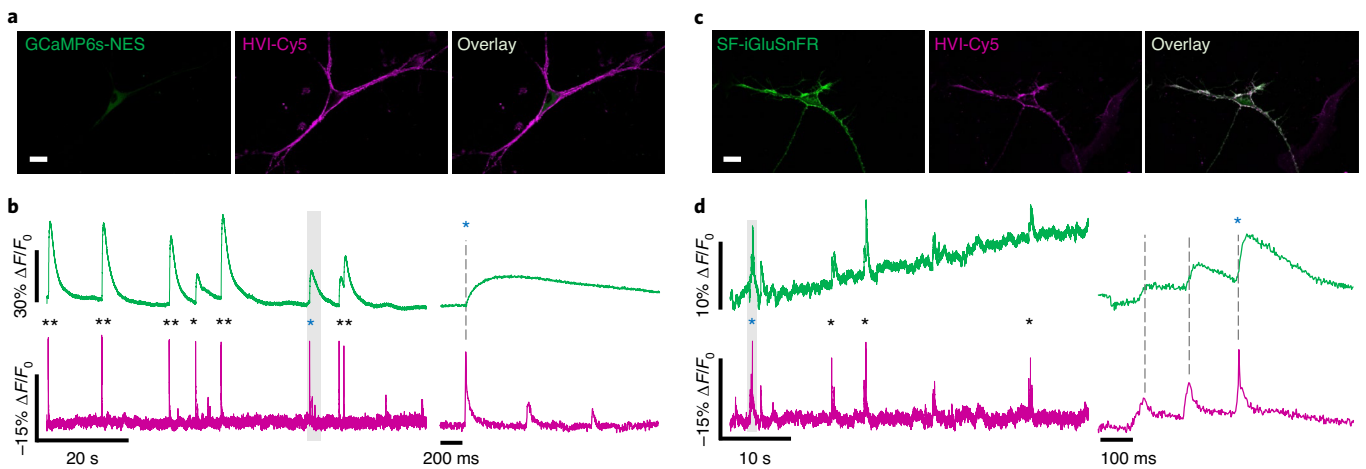

Fig. 4 | Multiplexed imaging with far-red HVI-Cy5 and green fluorescent indicators. a, Representative confocal images of a neuron co-expressing GCaMP6s-NES and HVI-Cy5. **b**, Dual-colour imaging of calcium (green) and voltage (magenta) at 484 Hz, with a zoomed-in view of the shaded region shown on the right. **c**, Representative confocal images of a neuron co-expressing SF-iGluSnFR and HVI-Cy5. **d**, Dual-colour imaging of glutamate (green) and voltage (magenta) at 484 Hz, with a zoomed-in view of the shaded region shown on the right. Cy5 traces have been corrected for photobleaching. Individual APs are marked with asterisks. Scale bars, 20 μm.

lular glutamate (Fig. 4c,d and Extended Data Fig. 6). In neurons co-expressing HVI-Cy5 and the green calcium indicator GCaMP6s in the cytoplasm (Fig. 4a), we observed time-correlated calcium spikes and AP spikes (Fig. 4b). The amplitudes of the calcium spikes were positively correlated with the number of AP spikes during burst AP activities, and subthreshold voltage activities did not lead

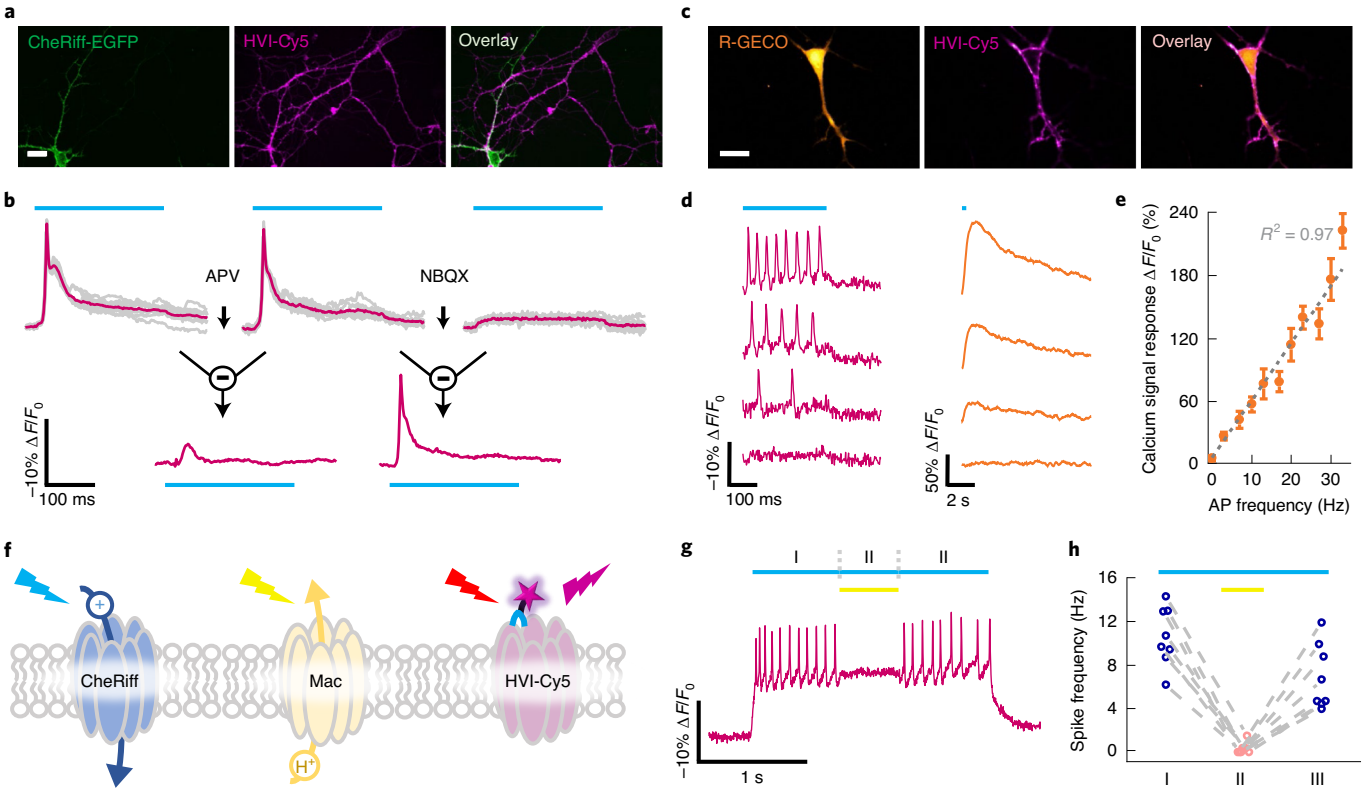

Fig. 5 | All-optical electrophysiology with HVI-Cy5. a, Representative confocal images of rat hippocampal neurons differentially expressing CheRiff-EGFP or HVI-Cy5. **b**, Top: pulsed blue-light illumination (250 ms, 0.3 W cm^{-2}) of the CheRiff-expressing neuron evokes AP firing in its neighbouring neuron expressing HVI-Cy5. The optical trace (10 trials superimposed) recorded under 637 nm laser illumination (0.6 W cm^{-2}) reports the membrane voltage of the same cell before (left) and after successive addition of 25 mM APV (middle) and 10 mM NBQX (right). APV and NBQX are blockers for the *N*-methyl-D-aspartate (NMDA) receptor and α-amino-3-hydroxy-5-methyl-4-isoxazolepropionic acid (AMPA) receptor, respectively. Bottom: the NMDA receptor-dependent fraction of postsynaptic potential is calculated as the difference between the fluorescence traces before and after APV addition. Similarly, the AMPA receptor-dependent fraction of postsynaptic potential is calculated as the difference between the fluorescence traces before and after NBQX addition. This pharmacological experiment was repeated twice. **c**, Representative confocal images of a neuron co-expressing R-GECO1, CheRiff and HVI-Cy5. **d**, Dual-colour imaging of voltage (left) and calcium (right) at 484 Hz on increasing the levels of blue-light stimulation (301-ms pulses from a 488 nm laser at 3, 5, 10 and 13 mW cm^{-2}). **e**, A linear regression of the calcium signal versus recorded AP frequencies. $n = 13$, 10, 7, 10, 6, 11, 9, 5, 5, 5 and 3 cells, respectively. Error bars represent s.e.m. **f**, Scheme of bidirectional control and imaging of membrane voltage in cells co-expressing CheRiff, Mac, and HVI-Cy5. **g**, Voltage imaging with HVI-Cy5 when AP spike trains evoked by 488 nm light illumination (0.03 W cm^{-2}) were interrupted by a 561 nm light pulse (0.5 W cm^{-2}). **h**, Correlation between spike frequency and optogenetic illumination ($n = 8$ cells). Scale bars, 20 μm.

to changes in the calcium signal (Fig. 4b). By contrast, the intracellular pH signal was not correlated with HVI-Cy5 dynamics under identical imaging conditions (Extended Data Fig. 6).

In neurons co-expressing HVI-Cy5 and the green glutamate sensor SF-iGluSnFR, both indicators trafficked well to the cell membrane (Fig. 4c). Similar to the observation for intracellular calcium, the occurrence of the extracellular glutamate signal was also time-correlated with the burst activities of AP spike trains, but the signal appeared spatially heterogeneous, probably due to localized glutamate release (Extended Data Fig. 6). The number of AP spikes in a cluster was positively correlated with the amplitude of the corresponding whole-cell-averaged glutamate signal. Low glutamate signal elicited subthreshold depolarization but failed to trigger AP firing (Fig. 4d). Together, our data demonstrate the power of HVI-Cy5 to enable multiplexed imaging of membrane potential with other physiological signals.

The far-red excitation spectrum of HVI-Cy5 also enabled pairing with optogenetic actuators. We combined HVI-Cy5 with a blue-light-activated cation channel, CheRiff[10], to achieve all-optical electrophysiology, where the membrane potential could be controlled and measured by different coloured light. When CheRiff and the HVI were co-expressed in the same rat hippocampal neuron, pulsed blue-light illumination at 0.1–0.3 W cm^{-2} triggered AP spike trains, which could be reported by HVI-Cy5 with SNRs of 35.4 ± 8.0 ($n = 6$ cells) and 15.6 ± 2.3 ($n = 4$ cells) under ~0.6 W cm^{-2} of 637 nm laser illumination at bandwidths of 464 Hz and 821 Hz, respectively (Extended Data Fig. 7). When CheRiff and HVI-Cy5 were differentially expressed in distinct neurons (Methods and Fig. 5a), blue-light stimulation of a CheRiff-expressing neuron could induce AP firing in a neighbouring neuron expressing HVI-Cy5. Consistent with the model of synaptic transmission, AP firing could be specifically blocked by 10 μM NBQX, an AMPA receptor inhibitor, whereas the addition of 25 μM APV, an NMDA receptor inhibitor, caused little change in the AP waveform (Fig. 5b).

We then extended this all-optical electrophysiology approach to simultaneously image membrane potential and calcium under various optogenetic stimulation dosages (3–38 mW cm^{-2}). In cultured neurons co-expressing HVI-Cy5, CheRiff and the red calcium indicator R-GECO1 (Fig. 5c), we observed concurrently higher AP firing frequencies and higher calcium signal levels upon increasing blue-light stimulation (Fig. 5d). Quantitative analysis revealed that the calcium signal was in direct proportion to the AP frequency

(~5.4 ± 0.3% R-GECO1 $\Delta F/F_0$ per Hz (mean ± s.e.m.); Fig. 5e). Little crosstalk was observed among the channels (Extended Data Fig. 8 and Supplementary Table 7).

Finally, we achieved simultaneous optical recording and bidirectional optical manipulation of the membrane potential. When HVI-Cy5, CheRiff and a yellow light-sensitive proton pump—Mac rhodopsin[45]—were co-expressed in the same neuron (Fig. 5f), blue-laser-stimulated AP spike trains were interrupted by pulsed yellow-light illumination (Fig. 5g,h). Thus, HVI-Cy5 enables low-crosstalk, all-optical electrophysiology that matches previous electrode-based approaches to investigate neuronal excitability (Extended Data Fig. 8).

Discussion

To summarize, we have employed site-specific protein modification to develop a panel of fast and sensitive genetically targetable voltage indicators, including a far-red hybrid indicator, HVI-Cy5. Among these, the sensitive and photostable HVI-Cy3 indicator exhibited the highest voltage sensitivity towards AP spikes (−25.3 ± 0.8 $\Delta F/F_0$ per AP), enabling voltage imaging at the single neuron level across a wide field of view and over an extended period of time (10 min). The bright and far-red HVI-Cy5 indicator is capable of reporting neuronal APs under a modest illumination intensity (0.2–1.2 W cm^{-2})—that is, ~100-fold lower than previous GEVIs with a similar emission spectrum (for example, Archon1)[10,14]. Taking advantage of its high sensitivity and redshifted spectrum, we have demonstrated the power of multiplexed imaging and all-optical electrophysiology with HVI-Cy5 in cultured neurons.

Compared to the spectrally similar indicator Voltron$_{635}$, the voltage sensitivity of HVI-Cy5 is 3.6-fold higher in reporting APs in cultured neurons (Table 1 and Supplementary Table 4)[24]. Although both the HVI and Voltron capitalize on the electrochromic quenching mechanism to report membrane voltage with a small-molecule fluorophore, they differ in their choices of protein–dye conjugation methods. In Voltron, the fluorophore is attached to the 34-kDa self-labelling protein tag fused to Ace2 rhodopsin, whereas in the HVIs, the fluorophore is directly linked to a 13-amino-acid peptide (1.6 kDa) inserted at the extracellular loop of the rhodopsin. The superior sensitivity of the HVIs over Voltron can be explained by the mechanism of voltage-dependent electrochromic quenching, in which voltage sensitivity is higher when the donor–quencher distance is shorter, all else being equal[28].

Notably, although HVI-Cy5 in its current form is mainly suitable for imaging cultured neurons, the in vitro cell culture system is an important complement to in vivo systems for studying molecular and cellular neuroscience. For example, voltage imaging assays in cell culture may assist in evaluating the effects of drugs on neuronal excitability in a higher-throughput and more cost-effective manner than the in vivo system[46]. As demonstrated in this study, the combination of HVI-Cy5 voltage imaging, optogenetic stimulation and drug perturbation has helped dissect the contributions of two glutamate receptor subtypes to synaptic transmission. Such an assay may be extended to high-throughput compound screening for receptor agonist and antagonist candidates.

From the bioorthogonal engineering perspective, the modular design of HVIs has the advantage of allowing the separate optimization of conjugation methods, rhodopsin scaffolds and fluorescence reporters. Our work has further demonstrated the safety, biocompatibility and fast reaction kinetics of IEDDA in the context of cultured neurons. A redshift in rhodopsin absorption has been reported previously in an Asp81Ser mutation[3,47]. Owing to the structural similarity between serine and cysteine, it is likely that the high voltage sensitivity of HVI-Cy5 also benefits from a redshifted rhodopsin absorption. Although HVI-Cy5 appears to photobleach more quickly than Voltron$_{635}$[24], this difference in photostability is mainly due to the dye performance (Cy5 versus JF 635) rather than the design of the HVIs, which is compatible with many organic fluorophore structures, as demonstrated by the palette of HVIs presented in this study (Fig. 2 and Supplementary Table 3). Because tetrazine-conjugated JF 635 is not commercially available, we chose mTz-Cy5 in this study to demonstrate the high voltage sensitivity and capability of multiplexed voltage imaging with HVIs. Future efforts would include replacing Cy5 with brighter and more photostable far-red organic fluorophores. Finally, to fully take advantage of voltage imaging in the far-red spectrum, future development of HVIs should focus on co-expressing the *trans*-cyclooctene ligase in the secretory pathway to metabolically label the Ace2 mutant within the cell. This approach has proven successful in cultured mammalian cells[48] and should open the door to in vivo applications of HVIs.

Online content

Any methods, additional references, Nature Research reporting summaries, source data, extended data, supplementary information, acknowledgements, peer review information; details of author contributions and competing interests; and statements of data and code availability are available at https://doi.org/10.1038/s41557-021-00641-1.

Received: 1 February 2020; Accepted: 15 January 2021;
Published online: 15 April 2021

References

1. Xu, Y. X., Zou, P. & Cohen, A. E. Voltage imaging with genetically encoded indicators. *Curr. Opin. Chem. Biol.* **39**, 1–10 (2017).
2. Gong, Y. Y. et al. High-speed recording of neural spikes in awake mice and flies with a fluorescent voltage sensor. *Science* **350**, 1361–1366 (2015).
3. Kannan, M. et al. Fast, in vivo voltage imaging using a red fluorescent indicator. *Nat. Methods* **15**, 1108–1116 (2018).
4. Jin, L. et al. Single action potentials and subthreshold electrical events imaged in neurons with a fluorescent protein voltage probe. *Neuron* **75**, 779–785 (2012).
5. Platisa, J., Vasan, G., Yang, A. & Pieribone, V. A. Directed evolution of key residues in fluorescent protein inverses the polarity of voltage sensitivity in the genetically encoded indicator ArcLight. *ACS Chem. Neurosci.* **8**, 513–523 (2017).
6. St-Pierre, F. et al. High-fidelity optical reporting of neuronal electrical activity with an ultrafast fluorescent voltage sensor. *Nat. Neurosci.* **17**, 884–889 (2014).
7. Abdelfattah, A. S. et al. A bright and fast red fluorescent protein voltage indicator that reports neuronal activity in organotypic brain slices. *J. Neurosci.* **38**, 3147–3148 (2018).
8. Yang, H. H. et al. Subcellular imaging of voltage and calcium signals reveals neural processing in vivo. *Cell* **166**, 245–257 (2016).
9. Hou, J. H., Kralj, J. M., Douglass, A. D., Engert, F. & Cohen, A. E. Simultaneous mapping of membrane voltage and calcium in zebrafish heart in vivo reveals chamber-specific developmental transitions in ionic currents. *Front. Physiol.* **5**, 344 (2014).
10. Hochbaum, D. R. et al. All-optical electrophysiology in mammalian neurons using engineered microbial rhodopsins. *Nat. Methods* **11**, 825–833 (2014).
11. Fan, L. Z. et al. All-optical synaptic electrophysiology probes mechanism of ketamine-induced disinhibition. *Nat. Methods* **15**, 823–831 (2018).
12. Adam, Y. et al. Voltage imaging and optogenetics reveal behaviour-dependent changes in hippocampal dynamics. *Nature* **569**, 413–417 (2019).
13. Flytzanis, N. C. et al. Archaerhodopsin variants with enhanced voltage-sensitive fluorescence in mammalian and *Caenorhabditis elegans* neurons. *Nat. Commun.* **5**, 4894 (2014).
14. Piatkevich, K. D. et al. A robotic multidimensional directed evolution approach applied to fluorescent voltage reporters. *Nat. Chem. Biol.* **14**, 352–360 (2018).
15. Zou, P. et al. Bright and fast multicoloured voltage reporters via electrochromic FRET. *Nat. Commun.* **5**, 4625 (2014).
16. Owen, S. F., Liu, M. H. & Kreitzer, A. C. Thermal constraints on in vivo optogenetic manipulations. *Nat. Neurosci.* **22**, 1061–1065 (2019).
17. Huang, Y. L., Walker, A. S. & Miller, E. W. A photostable silicon rhodamine platform for optical voltage sensing. *J. Am. Chem. Soc.* **137**, 10767–10776 (2015).
18. Fluhler, E., Burnham, V. G. & Loew, L. M. Spectra, membrane binding, and potentiometric responses of new charge shift probes. *Biochemistry* **24**, 5749–5755 (1985).

19. Treger, J. S., Priest, M. F., Iezzi, R. & Bezanilla, F. Real-time imaging of electrical signals with an infrared FDA-approved dye. *Biophys. J.* **107**, L9–L12 (2014).
20. Yan, P. et al. Palette of fluorinated voltage-sensitive hemicyanine dyes. *Proc. Natl Acad. Sci. USA* **109**, 20443–20448 (2012).
21. Grenier, V., Walker, A. S. & Miller, E. W. A small-molecule photoactivatable optical sensor of transmembrane potential. *J. Am. Chem. Soc.* **137**, 10894–10897 (2015).
22. Liu, P., Grenier, V., Hong, W., Muller, V. R. & Miller, E. W. Fluorogenic targeting of voltage-sensitive dyes to neurons. *J. Am. Chem. Soc.* **139**, 17334–17340 (2017).
23. Grenier, V., Daws, B. R., Liu, P. & Miller, E. W. Spying on neuronal membrane potential with genetically targetable voltage indicators. *J. Am. Chem. Soc.* **141**, 1349–1358 (2019).
24. Abdelfattah, A. S. et al. Bright and photostable chemigenetic indicators for extended in vivo voltage imaging. *Science* **365**, 699–704 (2019).
25. Uttamapinant, C. et al. Fast, cell-compatible click chemistry with copper-chelating azides for biomolecular labeling. *Angew. Chem. Int. Ed.* **51**, 5852–5856 (2012).
26. Yao, J. Z. et al. Fluorophore targeting to cellular proteins via enzyme-mediated azide ligation and strain-promoted cycloaddition. *J. Am. Chem. Soc.* **134**, 3720–3728 (2012).
27. Liu, D. S. et al. Diels–Alder cycloaddition for fluorophore targeting to specific proteins inside living cells. *J. Am. Chem. Soc.* **134**, 792–795 (2012).
28. Xu, Y. et al. Hybrid indicators for fast and sensitive voltage imaging. *Angew. Chem. Int. Ed.* **57**, 3949–3953 (2018).
29. Debets, M. F. et al. Bioconjugation with strained alkenes and alkynes. *Acc. Chem. Res.* **44**, 805–815 (2011).
30. Lukinavicius, G. et al. A near-infrared fluorophore for live-cell super-resolution microscopy of cellular proteins. *Nat. Chem.* **5**, 132–139 (2013).
31. Nikic, I. et al. Minimal tags for rapid dual-color live-cell labeling and super-resolution microscopy. *Angew. Chem. Int. Ed.* **53**, 2245–2249 (2014).
32. Nikic, I., Kang, J. H., Girona, G. E., Aramburu, I. V. & Lemke, E. A. Labeling proteins on live mammalian cells using click chemistry. *Nat. Protoc.* **10**, 780–791 (2015).
33. Beliu, G. et al. Bioorthogonal labeling with tetrazine-dyes for super-resolution microscopy. *Commun. Biol.* **2**, 261 (2019).
34. Versteegen, R. M., Rossin, R., ten Hoeve, W., Janssen, H. M. & Robillard, M. S. Click to release: instantaneous doxorubicin elimination upon tetrazine ligation. *Angew. Chem. Int. Ed.* **52**, 14112–14116 (2013).
35. Li, J., Jia, S. & Chen, P. R. Diels–Alder reaction-triggered bioorthogonal protein decaging in living cells. *Nat. Chem. Biol.* **10**, 1003–1005 (2014).
36. Fan, X. et al. Optimized tetrazine derivatives for rapid bioorthogonal decaging in living cells. *Angew. Chem. Int. Ed.* **55**, 14046–14050 (2016).
37. Li, J. & Chen, P. R. Development and application of bond cleavage reactions in bioorthogonal chemistry. *Nat. Chem. Biol.* **12**, 129–137 (2016).
38. Carlson, J. C. T., Mikula, H. & Weissleder, R. Unraveling tetrazine-triggered bioorthogonal elimination enables chemical tools for ultrafast release and universal cleavage. *J. Am. Chem. Soc.* **140**, 3603–3612 (2018).
39. Kralj, J. M., Hochbaum, D. R., Douglass, A. D. & Cohen, A. E. Electrical spiking in *Escherichia coli* probed with a fluorescent voltage-indicating protein. *Science* **333**, 345–348 (2011).
40. Kralj, J. M., Douglass, A. D., Hochbaum, D. R., Maclaurin, D. & Cohen, A. E. Optical recording of action potentials in mammalian neurons using a microbial rhodopsin. *Nat. Methods* **9**, 90–95 (2012).
41. Maclaurin, D., Venkatachalam, V., Lee, H. & Cohen, A. E. Mechanism of voltage-sensitive fluorescence in a microbial rhodopsin. *Proc. Natl Acad. Sci. USA* **110**, 5939–5944 (2013).
42. Mujumdar, R. B., Ernst, L. A., Mujumdar, S. R., Lewis, C. J. & Waggoner, A. S. Cyanine dye labeling reagents: sulfoindocyanine succinimidyl esters. *Bioconjug. Chem.* **4**, 105–111 (1993).
43. Bennett, M. V. & Zukin, R. S. Electrical coupling and neuronal synchronization in the mammalian brain. *Neuron* **41**, 495–511 (2004).
44. Dhein, S. Gap junction channels in the cardiovascular system: pharmacological and physiological modulation. *Trends Pharmacol. Sci.* **19**, 229–241 (1998).
45. Chow, B. Y. et al. High-performance genetically targetable optical neural silencing by light-driven proton pumps. *Nature* **463**, 98–102 (2010).
46. Kiskinis, E. et al. All-optical electrophysiology for high-throughput functional characterization of a human iPSC-derived motor neuron model of ALS. *Stem Cell Rep.* **10**, 1991–2004 (2018).
47. Xu, Y. et al. Imaging neuronal activity with fast and sensitive red-shifted electrochromic FRET indicators. *ACS Chem. Neurosci.* **10**, 4768–4775 (2019).
48. Uttamapinant, C., Sanchez, M. I., Liu, D. S., Yao, J. Z. & Ting, A. Y. Site-specific protein labeling using PRIME and chelation-assisted click chemistry. *Nat. Protoc.* **8**, 1620–1634 (2013).

Methods

Materials and reagents. The reagents used in this study are summarized in Supplementary Table 8. ^{W37V}LplA and ^{W37I}LplA were expressed in *Escherichia coli* and purified according to a previously published method[48]. For chemical synthesis, 10-azidodecanoic acid (**Az-9**) and *rel*-(1R-4E-pR)-cyclooct-4-ene-1-yl-*N*-pentanoic acid carbamate (**4-TCO**, previously described as TCO2[27]) were synthesized as previously described[26,27].

Chemical synthesis.

Az-9

Synthesis of 10-azidodecanoic acid (**Az-9**)

The synthesis of **Az-9** has been described previously[26]. Sodium azide (0.5 g, 7.7 mmol) was added to 10 ml *N*,*N*-dimethylformamide (DMF) containing 10-bromodecanoic acid (1.2 g, 4.8 mmol). The reaction was allowed to proceed at room temperature overnight and then evaporated under reduced pressure. The residue was dissolved in 15 ml of 1 M HCl and extracted with ethyl acetate (15 ml) three times. The organic layer, dried using magnesium sulfate, was evaporated under vacuum. The crude product was purified by silica gel chromatography using 10–20% ethyl acetate in hexanes. Only 15 ml of eluent was evaporated to afford the product as a pale yellow oil (~0.15 g). ^{1}H NMR (400 MHz, $CDCl_3$, δ): 3.25 (t, J = 6.95 Hz, 2H), 2.35 (t, J = 7.49 Hz, 2H), 1.61 (m, 5H), 1.32 (m, 9H). ESI-MS(−) calculated for $C_{10}H_8N_3O_2^-$ $[M\text{-}H]^-$: 212.14; found: 212.36.

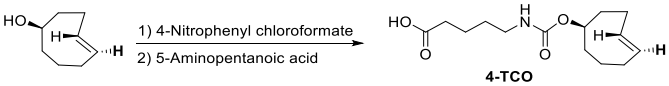

4-TCO

Synthesis of *rel*-(1R-4E-pR)-cyclooct-4-ene-1-yl-*N*-pentanoic acid carbamate (**4-TCO**)

The synthesis of **4-TCO** has been described previously[27]. The *rel*-(1R-4E-pR)-cyclooct-4-enol (0.5 g, 4.0 mmol) and pyridine (0.47 g, 6 mmol) were dissolved in dichloromethane and cooled at 0 °C. 4-Nitrophenyl chloroformate (0.96 g, 4.8 mmol) was added in multiple portions and the reaction was allowed to reach room temperature. The mixture was stirred in the dark for 3 h and poured into water (15 ml). The aqueous layer was extracted with diethyl ether (3 × 30 ml). The ether layer was combined, washed sequentially with aqueous acetic acid (pH 3, 3 × 30 ml), saturated aqueous $NaHCO_3$ (3 × 30 ml) and saturated aqueous NaCl (30 ml). The organic layer was dried over Na_2SO_4, filtered, and the solvent was removed to give *rel*-(1R-4E-pR)-cyclooct-4-ene-1-yl (4-nitrophenyl) carbonate as a light-yellow solid.

5-Aminopentanoic acid (0.7 g, 6 mmol) and diisopropylethylamine (DIPEA, 1.4 ml, 8 mmol) were dissolved in DMF (10 ml) and cooled at 0 °C. *rel*-(1R-4E-pR)-cyclooct-4-ene-1-yl (4-nitrophenyl) carbonate was added. The mixture was stirred at room temperature in the dark, overnight. The DMF was vaporized under reduced pressure and the resulting mixture was purified by column chromatography using 5:1 petroleum ether and ethyl acetate followed by 20:1 dichloromethane and methanol to obtain the *rel*-(1R-4E-pR)-cyclooct-4-ene-1-yl-*N*-pentanoic acid carbamate (**4-TCO**) as a colourless oil (0.7 g, 65%). ^{1}H NMR (400 MHz, CD_3OD, δ): 5.60–5.56 (m, 1H), 5.51–5.48 (m, 1H), 4.30–4.29 (m, 1H), 3.09 (t, J = 7.0 Hz, 2H), 2.37–2.28 (m, 5H), 2.00–1.89 (m, 4H), 1.75–1.67 (m, 2H), 1.64–1.57 (m, 3H), 1.53–1.47 (m, 2H). ^{13}C NMR (100 MHz, CD_3OD, δ): 177.35, 158.75, 136.10, 133.77, 81.57, 42.23, 41.23, 39.65, 35.18, 34.47, 33.49, 32.10, 30.42, 23.22. ESI-MS(+) calculated for $C_{28}H_{46}N_2NaO_8^+$, $[2M + Na]^+$: 561.31; found: 561.41. ESI-MS(−) calculated for $C_{28}H_{45}N_2NaO_8^-$, $[2M\text{-}H]^-$: 537.32; found: 537.58.

Molecular cloning. Plasmids were constructed using the Gibson assembly method. Briefly, the inserts and the vector were polymerase chain reaction (PCR) amplified into linear double-stranded DNA with overlapping sequences at the ends. These DNA fragments were mixed with Gibson assembly enzymes following the manufacturer's instructions (New England Biolabs). Successful clones were verified by sequencing. Site-directed mutagenesis and linker insertion/deletion were achieved by PCR-amplifying the vector with a pair of primers containing the desired mutation/insertion/deletion. The CheRiff gene was a gift from A. Cohen at Harvard University. The GCaMP6s, SF-iGluSnFR and ecliptic pHluorin genes were provided by Y. Li at Peking University. The R-GECO1 gene was from H. Cheng at Peking University. The Mac gene was a gift from L. Brown from the University of Guelph. Primers used in this study are listed in Supplementary Table 9.

Cell culture and transfection. HEK293T cells were incubated in Dulbecco's modified Eagle medium (DMEM, Gibco) containing 10% vol/vol fetal bovine serum (FBS, Gibco) at 37 °C with 5% CO_2. Cells were seeded in a 24-well plate and grown to 70–90% confluent for transfection. For each well, 500 ng plasmid and 1 µl Lipofectamine 2000 reagent were mixed in Opti-MEM medium and incubated for 15 min at room temperature. The mixture was added to the cell culture medium in the absence of serum for 4 h. Thereafter, cells were digested by trypsin-EDTA (0.25%, Gibco), reseeded on a sterile 14-mm glass coverslip pre-treated with matrigel matrix, and incubated in complete medium for 24 h before PRIME labelling.

For primary rat hippocampal neuron culture, sterile 14-mm glass coverslips were incubated with 20 µg ml^{-1} poly-D-lysine (Sigma) solution at 37 °C with 5% CO_2 for 24 h in a 24-well plate. The coverslips were washed twice with ddH_2O and incubated with 10 µg ml^{-1} laminin mouse protein (Gibco) solution at 37 °C with 5% CO_2 overnight. Thereafter, the coverslips were washed twice with ddH_2O and allowed to dry at room temperature. To isolate neurons, heads were separated from neonatal Sprague–Dawley rat pups with scissors. The brain was dissected from the skull and placed into a 35-mm dish with ice-chilled dissection solution (DMEM with high glucose and penicillin-streptomycin antibiotics). The hippocampus was isolated from the brains under a dissection scope, cut into small pieces (~0.5 mm) and incubated with 2 ml of Trypsin-EDTA (0.25%, Gibco) at 37 °C with 5% CO_2 for 15 min. The liquid was carefully aspirated and replaced with 1 ml of DMEM containing 10% FBS. The tissue fragments were dispersed by repeated pipetting for 1 min and incubated on ice for 5 min. The sediment was discarded, and the supernatant was collected and diluted by neuronal culture medium (Neurobasal medium, B-27 supplement, GlutaMAX supplement and penicillin-streptomycin) to a final cell density of 6×10^4 cells ml^{-1}. A 1-ml volume of cell suspension was added to each well of a 24-well plate (with a pre-coated glass coverslip). Half of the neuron culture medium was replaced with fresh medium once every four days.

Neurons were transfected on DIV7–9 (7–9 days in vitro). For each well of a 24-well plate, 250–500 ng of plasmid DNA was mixed with 1 µl of Lipofectamine 3000 reagent in Neurobasal medium, before incubation with neurons for 45 min. The transfected neurons were labelled and imaged after 3–10 days. For wide-field imaging assays, dissociated hippocampal neurons were nucleofected with FCK-^{Asp81Cys}Ace2 following the manufacturer's protocol (Lonza V4XP-3024). For synaptic transmission assays, dissociated hippocampal neurons were separately nucleofected with FCK-^{Asp81Cys}Ace2 and FCK-CheRiff-EGFP and co-plated in a 1:1 ratio into a well of a 24-well plate containing a pre-coated coverslip at a density of 1.5×10^5 cells per well. The medium was replaced with 1 ml of fresh medium after 4 h. Half of the medium was replaced by fresh medium every four days.

PRIME labelling. For PRIME-SPAAC labelling[26], hippocampal neurons were transfected with LAP-Ace(D81N) construct on DIV7–9 and labelled on DIV12–14. Transfected neurons were incubated with Tyrode's buffer containing 5 µM ^{W37I}LplA (purified from bacterial culture as previously described[48]), 500 µM **Az-9**, 2 mM ATP and 2 mM magnesium acetate for 30 min at 37 °C. Cells were rinsed three times with fresh Tyrode's buffer. The neurons were then incubated with Tyrode's buffer containing 10 µM DBCO-Cy3 for 10 min at 37 °C. Excess reagents were removed by buffer replacement, three times, with fresh Tyrode's buffer.

For PRIME-IEDDA labelling[27], transfected HEK293T cells or neurons were rinsed with Tyrode's salts solution (M&C Gene Technology) and then incubated with Tyrode's buffer containing 5 µM ^{W37V}LplA, 100 µM **4-TCO**, 1 mM ATP and 1 mM magnesium acetate for 30 min at 37 °C. Cells were gently rinsed with Tyrode's buffer three times, and subsequently labelled with 0.5 µM tetrazine dyes in Tyrode's buffer for 10 min. Excess reagents were removed from each well and cells were rinsed three times before the voltage imaging experiment.

Imaging apparatus and confocal microscopy. All of the fluorescence imaging experiments were conducted on an inverted fluorescence microscope (Nikon-TiE) equipped with a ×40, 1.3 NA oil immersion objective lens (except for wide-field imaging in Extended Data Fig. 5, which used a ×20, 1.05 NA dry objective lens), five laser lines (Coherent OBIS 488 nm, 532 nm, 561 nm, 594 nm and 637 nm), a spinning disk confocal unit (Yokogawa CSU-X1) and two scientific CMOS cameras (Hamamatsu ORCA-Flash 4.0 v2). The microscope, lasers and cameras were controlled with custom-built software written in LabVIEW (National Instruments, 15.0 version) and could switch between confocal and wide-field imaging modes. For two-colour simultaneous imaging, a dual-view device (Photometrics DV2) was used to split the emission into green/red and far-red fluorescence channels. The spectra properties of the filters and dichroic mirrors for various fluorescent indicators used in this study are summarized in Supplementary Table 10. The transfected HEK293T cells or neurons on coverslips were transferred to Tyrode's buffer before imaging. Confocal images were acquired at 1 × 1 camera binning with an exposure time of 100 ms. Image analysis was performed in ImageJ/Fiji (version 1.52d).

Electrophysiology. For single-cell electrophysiology recording, cultured neurons were incubated in Tyrode's buffer containing 20 µM gabazine, 10 µM NBQX and 25 µM APV (Tyrode's buffer containing 50 nM 2-APB for HEK293T cells). The electrophysiology experiments were performed at room temperature. Borosilicate glass electrodes (Sutter) were pulled to a tip resistance of 2.5–5 MΩ. The glass electrode was filled with internal solution containing 125 mM potassium gluconate, 8 mM NaCl, 0.6 mM $MgCl_2$, 0.1 mM $CaCl_2$, 1 mM EGTA, 10 mM HEPES, 4 mM Mg-ATP, 0.4 mM GTP·Na_2 (pH 7.3) and adjusted to 295 mOsm kg^{-1} with 1 M sucrose. The glass electrode's position was adjusted by a Sutter MP285 micro-manipulator. The cells were clamped using an Axopatch 200B amplifier

(Axon Instruments). Membrane voltage signal recorded from the patch amplifier was filtered with an internal 5-kHz Bessel filter and digitized at 9,681.48 Hz with a National Instruments PCIe-6353 data acquisition (DAQ) board (approximately twice the bandwidth of the Bessel filter).

Simultaneous patch clamp and optical recording in HEK293T cells. The membrane potential of the HEK293T cells was controlled via whole-cell patch clamp (Axopatch 200B, Axon Instruments). To characterize the dynamic range and kinetics of the voltage indicators in HEK293T cells, the membrane potential was stepped from −100 mV to 100 mV in increments of 20 mV, with each step lasting 500 ms. Meanwhile, fluorescence images were recorded at a camera frame rate of 1,058 Hz.

To map gap junction-mediated electrical coupling, HEK293T cells at full confluence were labelled with Cy3 fluorophore via PRIME-IEDDA. To measure the decay length of electrical coupling, cell image series were acquired at a camera frame rate of 10 Hz with the membrane potential ramped between −100 mV and 50 mV for four cycles. To estimate the rate of electrical coupling, cell image series were acquired at a camera frame rate of 200 Hz with the membrane potential stepped between −70 mV and 30 mV.

Voltage imaging in rat hippocampal neuron culture. To stimulate firing of individual APs, current of 200–500 pA was injected to cultured neurons for 5–10 ms at a repetition rate of 250–500 ms. Alternatively, neurons were stimulated with current of 100–200 pA for 500 ms to fire AP spike trains. Fluorescence images were acquired at a camera frame rate of 484 Hz with 2×2 binning. For wide-field voltage imaging, fluorescence images from a field of view of 452 μm × 161 μm were recorded at 400 Hz for a total of 10 min.

For simultaneous imaging with GCaMP6s and HVI-Cy5, neurons were illuminated with 488 nm and 637 nm lasers at 1.3–2.5 W cm^{-2} and 0.5–1.2 W cm^{-2}, respectively, and continuously imaged for 80–100 s at a camera frame rate of 484 Hz. For simultaneous imaging with SF-iGluSnFR and HVI-Cy5, neurons were illuminated with 488 nm and 637 nm lasers at 0.6–1.9 W cm^{-2} and 0.2–0.5 W cm^{-2}, respectively, and continuously imaged for 50–100 s at a camera frame rate of 484 Hz.

CellTiter-Glo assay for cell viability. Cell viability was measured by CellTiter-Glo (Promega) assay, which quantified the cellular ATP levels. Neurons were plated in 96-well plates at 13,000 cells per well and cultured as described above. On DIV7–9, neurons were transfected with 125 ng of plasmid DNA per well by Lipofectamine 3000. On DIV12–14, neurons were labelled with 5 μM LplA and 100 μM **4-TCO** for 30 min, followed by 1 μM mTz-Cy5 for 10 min, as described above. Neurons were then illuminated with a xenon lamp equipped with a >650 nm long-pass filter at ~0.5 W cm^{-2} for 5 min. Thereafter, medium in each well was replaced with 100 μl Tyrode's buffer and 100 μl CellTiter-Glo reagent. The sample was mixed on an orbital shaker for 2 min before being maintained at room temperature for 10 min. Luminescence was recorded on a microplate reader (Synergy H4 hybrid multimode microplate reader). Eight technical replicates were performed for each sample.

All-optical electrophysiology with HVI-Cy5. Cultured rat hippocampal neurons expressing CheRiff and HVI-Cy5 were illuminated with 2-ms blue-light pulses at 0.13–0.31 W cm^{-2} to stimulate AP firing. Alternatively, cells were stimulated with 250 ms of blue-light illumination at 0.06–0.31 W cm^{-2} to fire AP spike trains. Fluorescence images were acquired at a camera frame rate of either 464 Hz or 821 Hz.

For the synaptic transmission assay, the differential expression of CheRiff and HVI was achieved by electroporating two pools of rat hippocampal neurons in suspension with two genes, respectively, before co-plating them together in the same cell cultural dish, as previously described in the 'Cell culture and transfection' section. Cultured neurons were imaged in Tyrode's buffer at a camera frame rate of 464 Hz. For each measurement, a 250-ms blue-light pulse (0.3 W cm^{-2}) was repeated 10 times under constant 637 nm illumination (0.2 W cm^{-2}). Subsequently, 25 μM APV was added to the Tyrode's buffer and the same measurement was repeated after 3 min. Thereafter, 10 μM NBQX was added to the buffer, followed by another round of measurements.

To simultaneously monitor intracellular calcium and membrane voltage in neurons undergoing optogenetic stimulation, rat hippocampal neurons were transfected with R-GECO1 and ^{Asp81Cys}Ace2-P2A-CheRiff, as previously described in the 'Cell culture and transfection' section. Neurons were stimulated by a 488 nm laser for 301 ms at 3, 5, 10 and 13 mW cm^{-2}, while continuously excited with 561 nm and 637 nm lasers at 0.1 W cm^{-2} and 0.2 W cm^{-2}, respectively, and imaged at a camera frame rate of 484 Hz. The R-GECO1 data were smoothed and digitally resampled at 48.4 Hz to boost the SNR.

For the bidirectional optical control and recording of membrane potential, cultured rat hippocampal neurons were co-transfected with ^{Asp81Cys}Ace2 and Mac-P2A-CheRiff at a 2:1 ratio and labelled with Cy5 as described above. Neurons were illuminated with a 637 nm laser at 0.2 W cm^{-2} and imaged at a camera frame rate of 464 Hz. For optogenetic control, neurons were activated with 488 nm laser illumination at 0.03–0.12 W cm^{-2} and deactivated with 561 nm laser illumination at 0.5 W cm^{-2}.

Photocurrent measurements. Cultured rat hippocampal neurons were transfected with HVI or VARNAM constructs as previously described. Photocurrent measurements were performed in Tyrode's buffer containing 20 μM gabazine, 10 μM NBQX and 25 μM APV to block synaptic transmission, and 500 nM tetrodotoxin (TTX) to block AP firing. On DIV12–14, cells expressing HVI were labelled with fluorophores and voltage-clamped at −70 mV via a patch pipette. The photocurrent was measured with a DAQ and digitized at 20 kHz when cells were illuminated with 300-ms laser pulses at the following intensities: HVI-488, 488 nm, 3.1 W cm^{-2}; HVI-Cy3, 532 nm, 4.9 W cm^{-2}; VARNAM, 561 nm, 4.8 W cm^{-2}; HVI-594, 594 nm, 3.8 W cm^{-2}; HVI-Cy5, 637 nm, 0.48 W cm^{-2}.

Data analysis. Both the electrical data and the fluorescence images were analysed with home-built software written in MATLAB (MathWorks, version R2018b). For each labelled cell, fluorescence intensities were extracted from the mean pixel values of a manually drawn region of interest around the soma. Following camera bias subtraction (100 and 400 for 1×1 and 2×2 binning, respectively), the fluorescence signal was corrected for photobleaching. The optical traces in Fig. 5g and Extended Data Fig. 8 were corrected for yellow-light-induced Cy5 fluorescence (4.0% under our illumination conditions). This level of optical crosstalk was determined by the experiments described in Extended Data Fig. 8. Statistical analysis was performed with Excel (Microsoft Excel 2019) and Origin (version 2019b).

Reporting Summary. Further information on research design is available in the Nature Research Reporting Summary linked to this Article.

Data availability

All relevant data presented in this study are provided in the Article, Extended Data figures and Supplementary Information. The data and genetic constructs are also available from the corresponding authors upon request.

Code availability

MATLAB code can be downloaded from GitHub at https://github.com/PKUCHEMZouLab/HVI. Alternatively, it is available from the corresponding authors upon request.

Acknowledgements

We acknowledge funding from the Ministry of Science and Technology (2018YFA0507600, 2017YFA0503600 and 2016YFA0501500), the National Natural Science Foundation of China (91753131, 32088101, 21673009, 21521003 and 21937001), the Natural Science Foundation of Beijing Municipality (5182011) and the Interdisciplinary Medicine Seed Fund of Peking University (BMU2017MC006). P.Z. was sponsored by a Li Ge-Zhao Ning Life Science Junior Research Fellowship, a Bayer Investigator Award and a National Thousand Young Talents Award. P.R.C. is the recipient of the XPLORER PRIZE from the Tencent Foundation. We thank Y. Li, H. Cheng, A. Cohen and L. Brown for providing plasmids. Z. Wu and Y. Li helped provide rat hippocampal neurons.

Author contributions

P.Z. and P.R.C. conceived and supervised the project. S.L., C.L., Y.X. and L.P. performed all experiments, unless otherwise noted. C.L. and H.L. carried out chemical syntheses. X.Z. assisted with neuron culture. H.Z. assisted with purification of plasmids and enzymes. S.L., C.L., P.R.C. and P.Z. analysed data. S.L., C.L. and P.Z. wrote the manuscript with input from all authors.

Competing interests

The authors declare no competing interests.

Additional information

Extended data is available for this paper at https://doi.org/10.1038/s41557-021-00641-1.

Supplementary information The online version contains supplementary material available at https://doi.org/10.1038/s41557-021-00641-1.

Correspondence and requests for materials should be addressed to P.R.C. or P.Z.

Peer review information *Nature Chemistry* thanks the anonymous reviewers for their contribution to the peer review of this work.

Reprints and permissions information is available at www.nature.com/reprints.

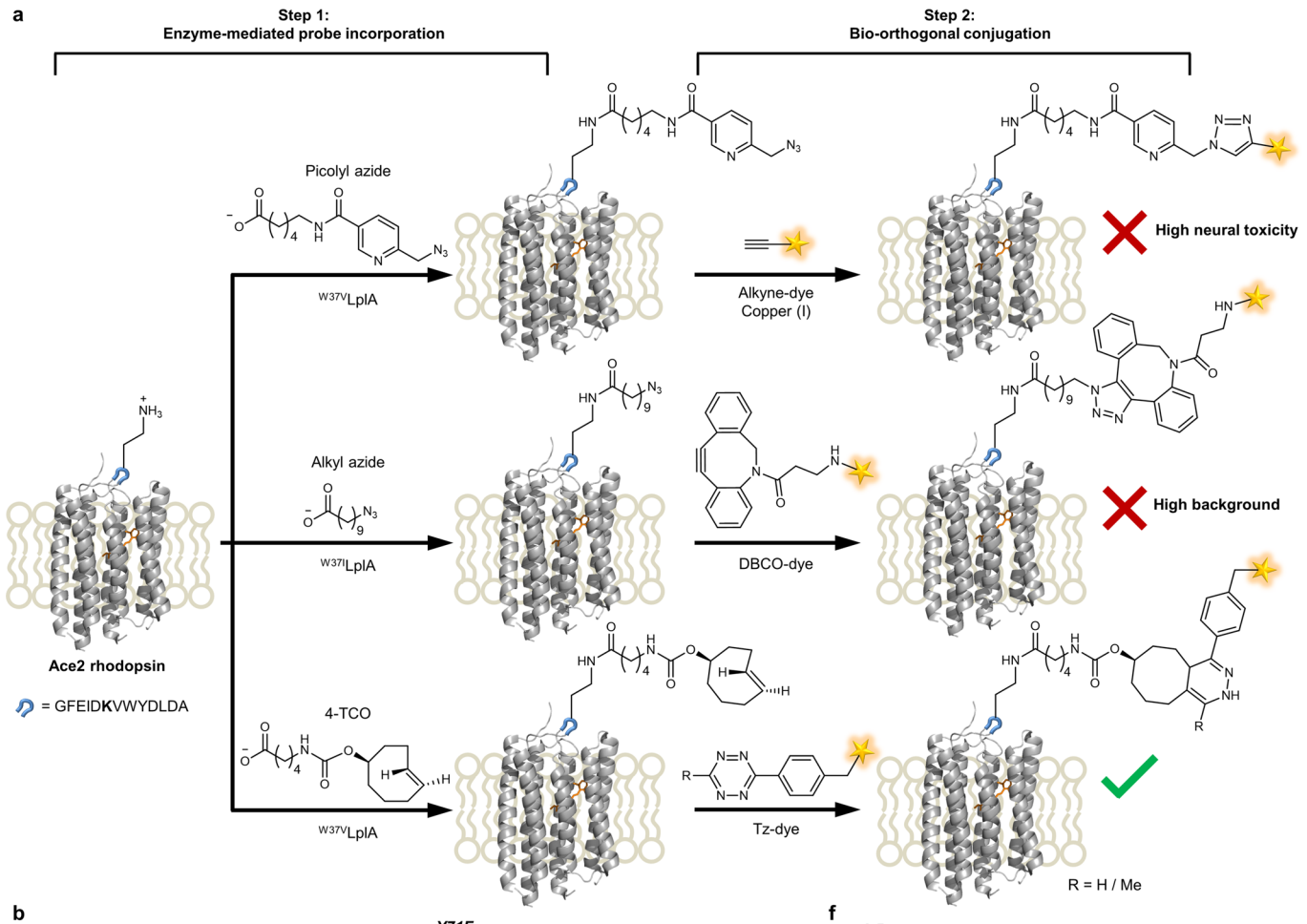

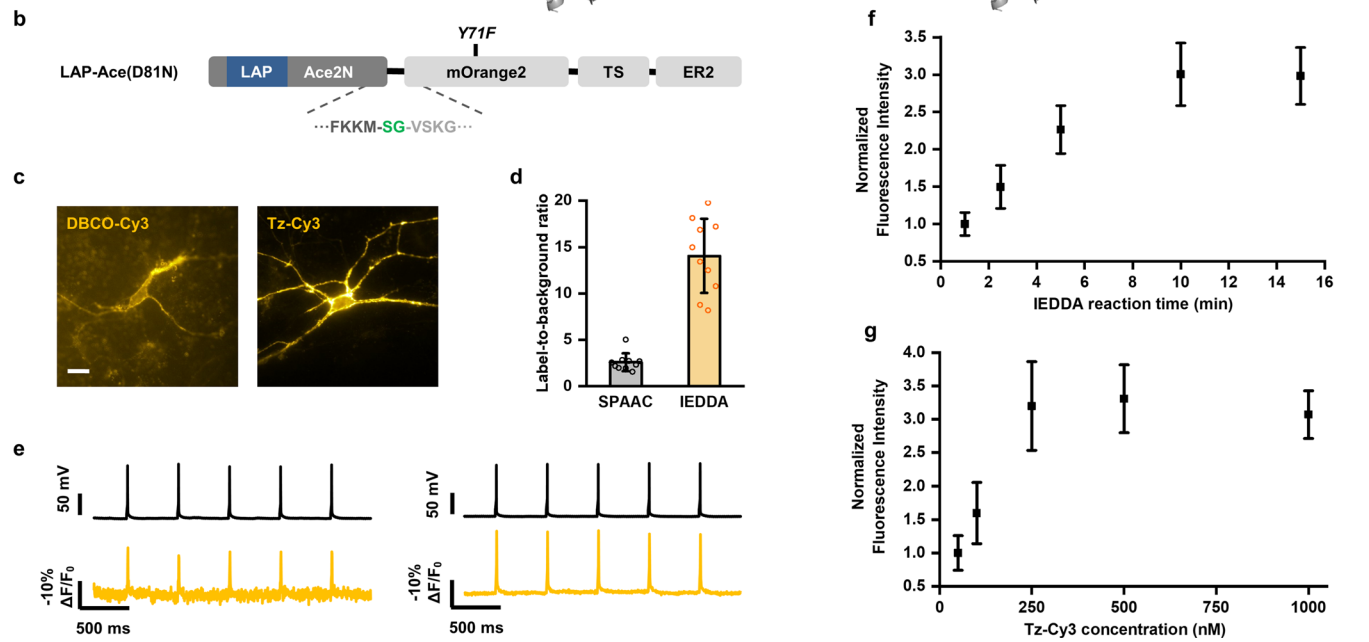

Extended Data Fig. 1 | See next page for caption.

Extended Data Fig. 1 | Optimization of site-specific membrane protein labeling strategy. a, Top: Probe incorporation mediated by enzyme (PRIME) coupled with copper-assisted alkyne-azide cycloaddition (CuAAC). Middle: PRIME coupled with strain-promoted alkyne-azide cycloaddition (SPAAC). Bottom: PRIME coupled with inverse-electron-demand Diels–Alder cycloaddition (IEDDA). **b**, LAP-Ace(D81N) domain structure. **c**, Representative confocal images of rat hippocampal neurons expressing LAP-Ace(D81N) and labeled with either DBCO-Cy3 (left) or Tz-Cy3 (right), scale bar = 20 μm. **d**, Label-to-background ratio of SPAAC and IEDDA conjugation methods. n = 10 and 10 cells, respectively. Error bars represent S.D. **e**, Simultaneous electrical and optical recording of stimulated action potentials from cultured neurons labeled with Cy3 via either SPAAC (left) or IEDDA (right). Cy3 traces were recorded from single trial measurements without temporal averaging. **f**,**g**, Cultured rat hippocampal neurons at DIV15-16 were labeled with 5 μM LplA and 100 μM 4-TCO for 30 min, before labeled with Tz-Cy3 via IEDDA at various probe concentrations and incubation times. (**f**) IEDDA labeling with 500 nM Tz-Cy3 for 1 to 15 min. n = 27 cells (1 min), 19 cells (2.5 min), 19 cells (5 min), 20 cells (10 min) and 22 cells (15 min). (**g**) IEDDA labeling for 10 min with 50 to 1000 nM Tz-Cy3. n = 13 cells (50 nM), 14 cells (100 nM), 18 cells (250 nM), 17 cells (500 nM) and 26 cells (1000 nM). Whole cell fluorescence intensities were measured on an inverted fluorescence microscope and normalized to either 1 min or 50 nM. Error bars represent s.e.m.

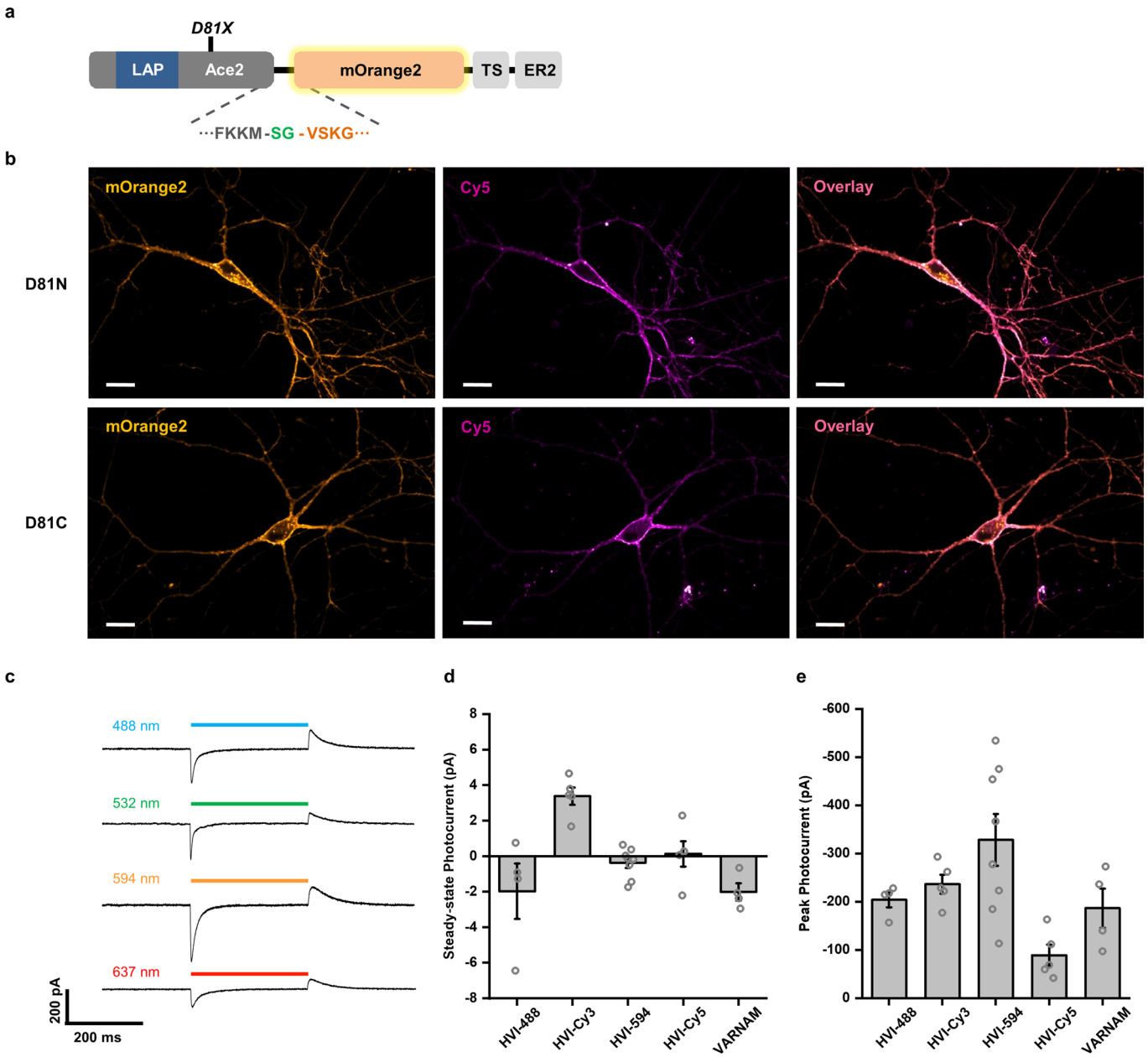

Extended Data Fig. 2 | Membrane trafficking and photocurrents of HVIs. a, LAP-Ace(D81X)-mOrange2 domain structure. **b**, Representative confocal images of cultured rat hippocampal neurons expressing to Ace(D81N) and Ace(D81C) mutants labeled with Tz-Cy5. Top: mOrange2 images showing the expression of Ace fusion. Middle: Cy5 images showing IEDDA fluorescence label. Bottom: overlay of mOrange2 and Cy5 channels. Scale bars = 20 μm. Photocurrent measurements were performed on DIV12–14. Cells expressing HVI were labeled with fluorophores and voltage-clamped at -70 mV via a patch pipet. **c**, Representative electrical traces of photocurrents in cultured neurons expressing HVI under a 300-ms light illumination pulse at laser wavelengths of 488 nm (3.1 W/cm^2, n = 4 cells), 532 nm (4.9 W/cm^2, n = 5 cells), 594 nm (3.8 W/cm^2, n = 8 cells) and 637 nm (0.48 W/cm^2, n = 5 cells), respectively. **d**,**e**, The steady-state photocurrents (**d**) and peak photocurrents (**e**) of HVIs and VARNAM (561 nm, 4.8 W/cm^2) in response to different laser wavelengths, measured in cultured rat hippocampal neurons. Error bars represent s.e.m.

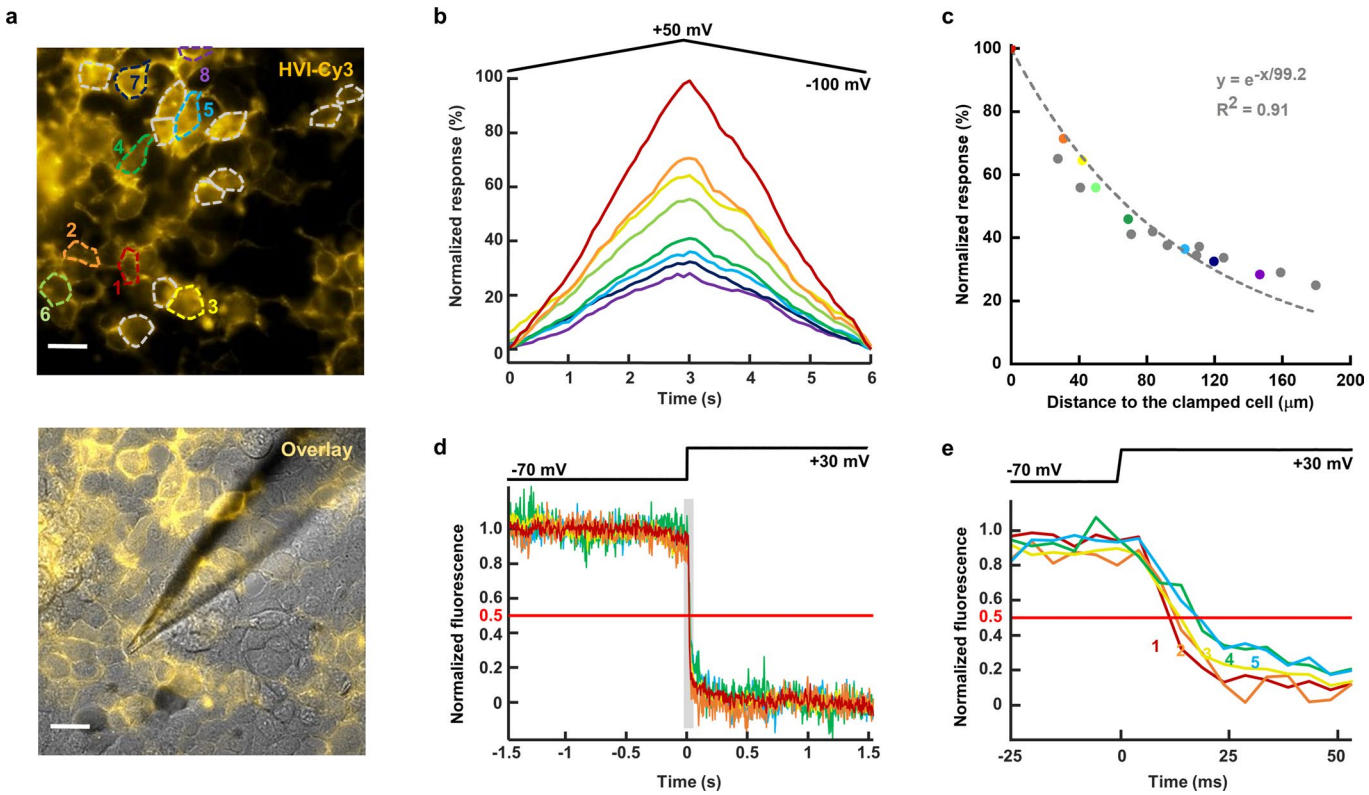

Extended Data Fig. 3 | Mapping electrical connectivity of cultured HEK293T cells. a, A representative 333 μm × 333 μm wide-field fluorescence image of HEK293T cells expressing HVI-Cy3 (top). An overlay of Cy3 fluorescence with DIC image is shown at the bottom. Scale bars = 20 μm. **b**, F-V response curves of cells indicated in **a**. The membrane potential of cell #1 (red) was controlled via whole-cell voltage clamp at 1000 Hz, and ramped between -100 mV to +50 mV. Fluorescence images of the whole field were acquired at a camera frame rate of 10 Hz. The fluorescence response had been normalized to cell #1. **c**, Single exponential fitting of normalized response versus the distance to the clamped cell (grey dashed line). The decay length constant is calculated to be 99.2 μm. **d**, Fluorescence response to step-wise voltage changes, similar to **b**, except that the membrane potential was stepped between -70 mV and 30 mV, while cells in a 166 μm × 166 μm field of view were imaged at 200 Hz camera frame rate. The fluorescence signals had been normalized to the fluorescence at V_m = -70 mV and 30 mV. **e**, A zoomed-in view of the shaded region in **d**, showing the normalized fluorescence response during a depolarization voltage step. The time point at step voltage change is defined as t = 0.

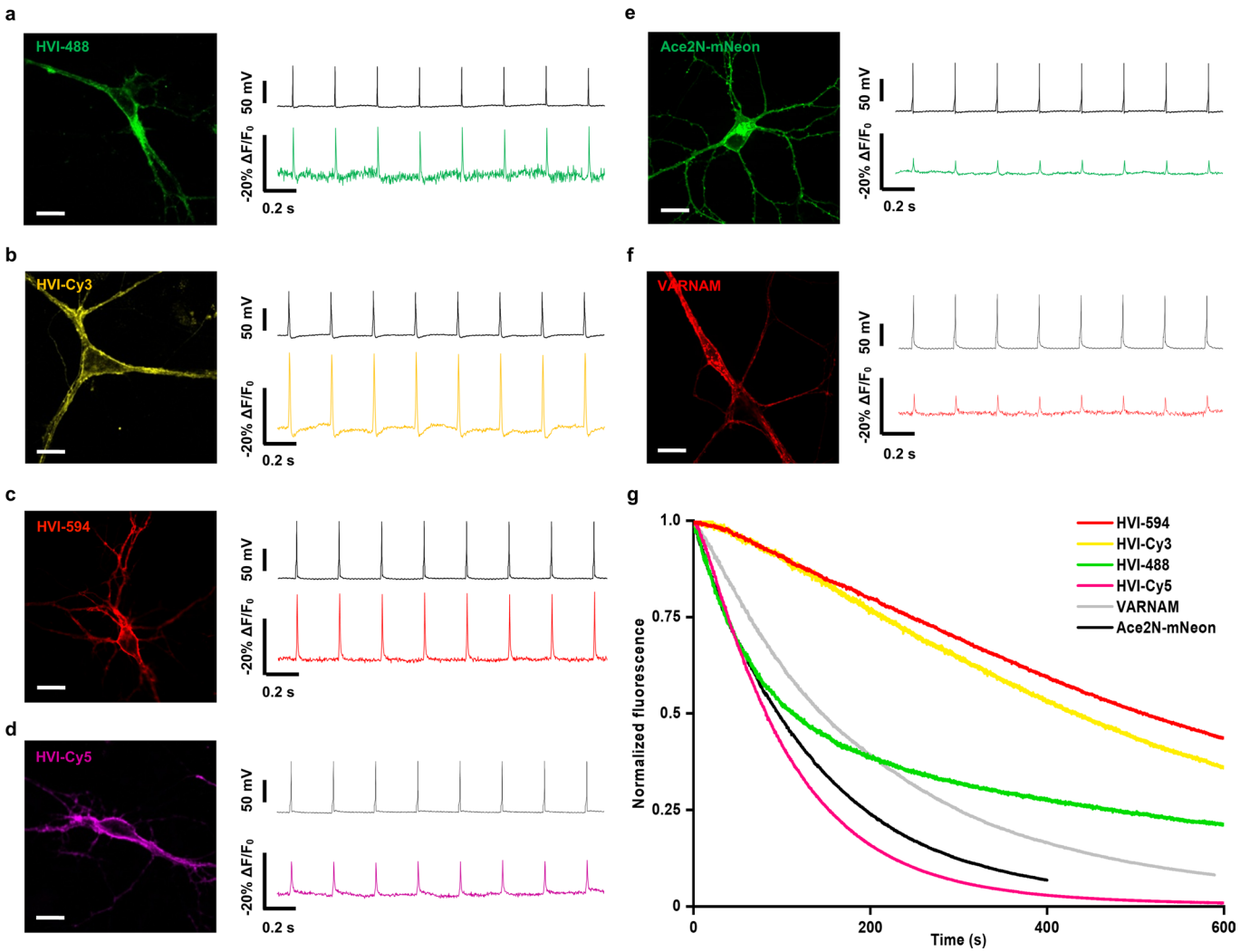

Extended Data Fig. 4 | Fluorescence images and photostability of a panel of voltage indicators. a-f, Left: representative confocal images of rat hippocampal neurons expressing HVI-488 (**a**), HVI-Cy3 (**b**), HVI-594 (**c**), HVI-Cy5 (**d**), Ace2N-mNeon (**e**), and VARNAM (**f**). Scale bars = 20 μm. Right: single trial recordings membrane voltage and fluorescence response of these indicators at 484 Hz camera frame rate. **g**, Representative photobleaching curves are shown for VARNAM, Ace2N-mNeon, and HVIs, measured in HEK293T cells. Photobleaching constants are summarized in Supplementary Table 6. Image sampling rate is 20 Hz. Fluorescence intensities were normalized to the initial value at t = 0.

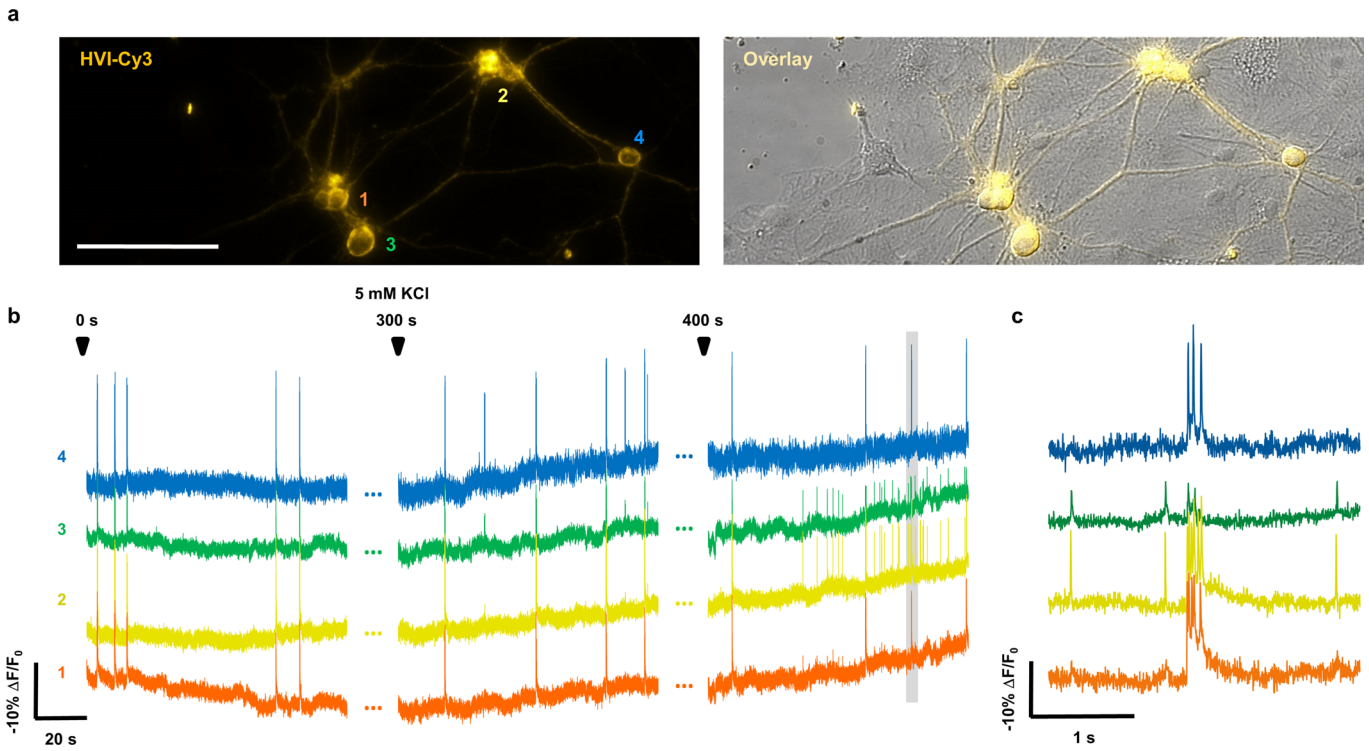

Extended Data Fig. 5 | Wide-field voltage imaging of multiple neurons with HVI-Cy3. a, A representative 452 μm × 161 μm wide-field image of cultured rat hippocampal neurons expressing HVI-Cy3 (left). An overlay with DIC image is shown on the right. Scale bars = 50 μm. **b**, Wide-field voltage imaging of HVI-Cy3 at 400 Hz over 10 min under ~2 W/cm^2 illumination with 20× NA1.05 dry objective lens. The fluorescence traces of four individual neurons are shown during the time window of 0-100 s, 300-400 s, and 400-500 s. At t = 300 s, 5 mM KCl was added to stimulate AP firing. **c**, A zoom-in view of the shaded region in **b**.

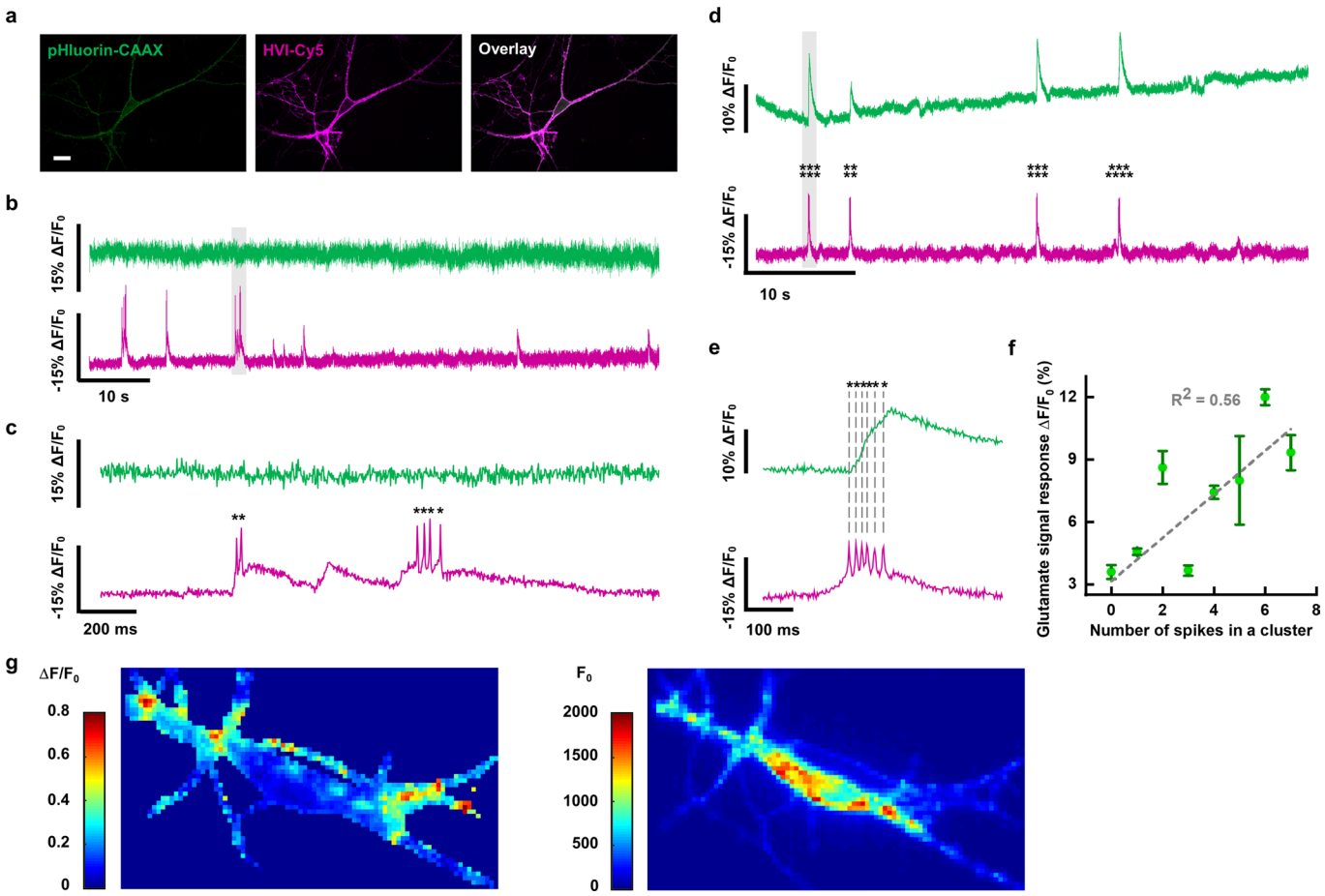

Extended Data Fig. 6 | Simultaneous dual-color imaging of pH or extracellular glutamate and membrane voltage in neurons. a, Representative confocal images of rat hippocampal neurons co-expressing a membrane-anchored pHluorin-CAAX (left) and HVI-Cy5 voltage indicator (middle). The overlay image of pHluorin and Cy5 is shown on the right. Scale bar = 20 μm. **b**, Dual-color imaging of pHluorin (green trace, 488 nm, 2.5 W/cm^2) and HVI-Cy5 (magenta trace, 637 nm, 0.9 W/cm^2) at 484 Hz for 100 s. The signals of pHluorin and Cy5 had been corrected for photobleaching. **c**, A zoom-in view of the shaded region in **b**. Individual APs are marked with asterisks. **d**, Glutamate (top) and membrane voltage (bottom) traces were monitored with SF-iGluSnFR and HVI-Cy5, respectively, at a camera frame rate of 484 Hz. **e**, A zoom-in view of the shaded region in **d**. Cy5 traces have been corrected for photobleaching. Individual APs are marked with asterisks. **f**, A linear regression of the glutamate signal versus the number of recorded AP spikes in clusters. n = 30, 21, 8, 6, 7, 2, 6, and 3 cells, respectively. Error bars represent s.e.m. **g**, Heatmap images at 8-by-8 binning showing the $\Delta F/F_0$ and baseline fluorescence (F_0) of SF-iGluSnFR during the time window indicated by the shaded region in **d**.

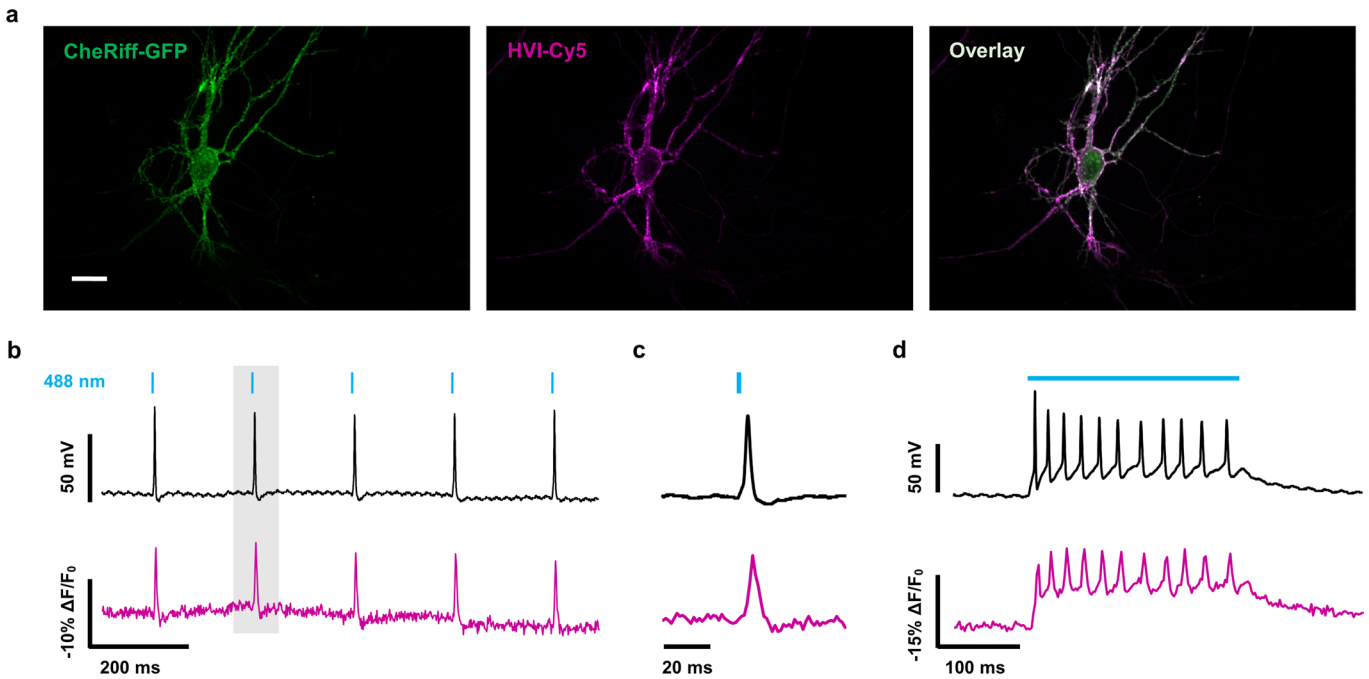

Extended Data Fig. 7 | All-optical electrophysiology with HVI-Cy5 with CheRiff. a, Representative confocal images of rat hippocampal neurons co-expressing CheRiff-EGFP and HVI-Cy5. Scale bar = 20 μm. **b**, Neurons were stimulated to fire individual APs upon illumination with 2-ms blue-light pulses. Membrane voltage and fluorescence responses were recorded simultaneously via patch pipette and camera at a frame of 821 Hz, respectively. **c**, A zoom-in view of the shaded region in **b**. **d**, Neurons were stimulated to fire AP spike trains via 250-ms blue-light illumination. Image sampling rate was 464 Hz.

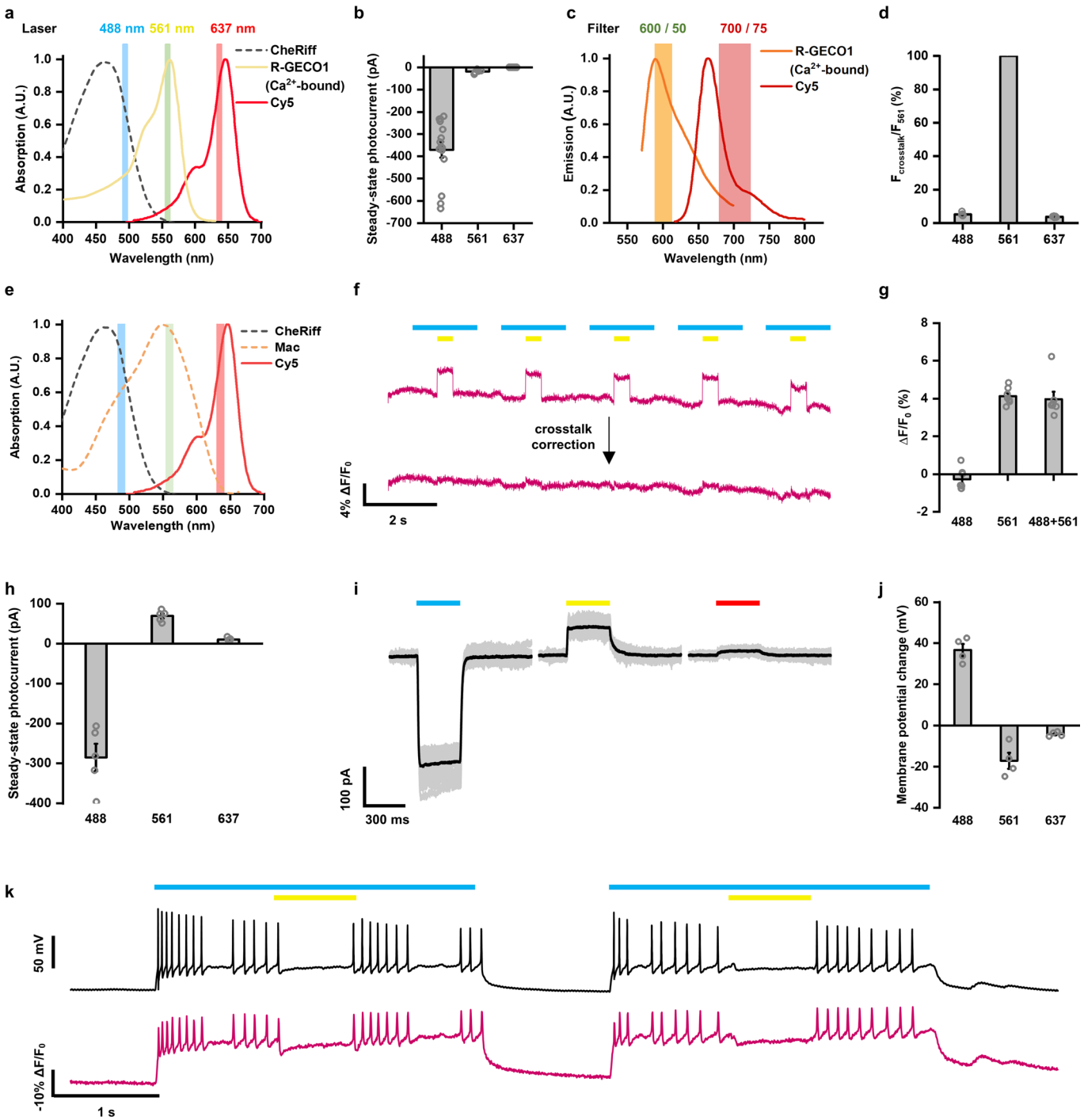

Extended Data Fig. 8 | See next page for caption.

Extended Data Fig. 8 | Characterization of optical and optogenetic crosstalk among HVI-Cy5, CheRiff, and R-GECO1 or Mac. a, Overlay of the absorption spectrum of CheRiff (dashed curve), and the excitation spectra of R-GECO1 (yellow) and Cy5 (red). Blue, yellow and red bars represent 488 nm, 561 nm and 637 nm laser lines respectively. **b**, Steady-state photocurrent generated by 488 nm (0.03 W/cm^2, -371 ± 35 pA, n = 15 cells), 561 nm (0.10 W/cm^2, -18.0 ± 3.4 pA, n = 6 cells) or 637 nm (0.36 W/cm^2, 0.0 ± 0.1 pA, n = 10 cells) in CheRiff-expressing neurons. **c**, The emission spectra of R-GECO1 (orange) and Cy5 (red). The emission filters used in this study are indicated as shaded regions. **d**, Neurons expressing R-GECO1 were illuminated by 488 nm (0.03 W/cm^2), 561 nm (0.10 W/cm^2) and 637 nm (0.36 W/cm^2), respectively. The optical crosstalk (measured with the emission filter 600/50) was normalized to 561 nm illumination (n = 6 neurons). Error bars represent s.e.m. **e**, Overlay of the action spectra of Mac[45] (grey dashed curve) and CheRiff[10] (orange dashed curve) and the excitation spectrum of Cy5 (red). Blue, yellow and red bars represent 488 nm, 561 nm and 637 nm laser lines, respectively. **f**, Representative HVI-Cy5 fluorescence trace of cultured neuron before and after 4.0% optical crosstalk correction (see below). Blue bar: 2153-ms 488 nm light illumination at 0.03 W/cm^2. Yellow bar: 538-ms 561 nm light illumination at 0.48 W/cm^2. Cy5 fluorescence was recorded under continuous 637 nm illumination at 0.24 W/cm^2. **g**, Whole-cell fluorescence changes of neurons expressing HVI-Cy5 under 488 nm and/or 561 nm laser illuminations. 561 nm illumination caused a 4.0% increase in Cy5 fluorescence, whereas 488 nm laser illumination had negligible effect (n = 7 neurons). **h**, Representative photocurrent traces over 30 repeated trails. **i**,**j**, Steady-state photocurrent (**i**, n = 5 cells) and membrane depolarization (**j**, n = 4 cells) generated by 488 nm (0.06 W/cm^2), 561 nm (0.48 W/cm^2) or 637 nm (0.24 W/cm^2) illumination of neurons expressing Mac-P2A-CheRiff. **k**, Simultaneous electrical and optical recordings of APs from a neuron co-expressing Mac-P2A-CheRiff and HVI-Cy5. Blue-light stimulation caused AP firing, which was interrupted by yellow light pulses. Error bars represent s.e.m.

nature research

Corresponding author(s): Peng Zou

Last updated by author(s): Aug 19, 2020

Reporting Summary

Nature Research wishes to improve the reproducibility of the work that we publish. This form provides structure for consistency and transparency in reporting. For further information on Nature Research policies, see our Editorial Policies and the Editorial Policy Checklist.

Statistics

For all statistical analyses, confirm that the following items are present in the figure legend, table legend, main text, or Methods section.

n/a	Confirmed	
☐	☒	The exact sample size (*n*) for each experimental group/condition, given as a discrete number and unit of measurement
☐	☒	A statement on whether measurements were taken from distinct samples or whether the same sample was measured repeatedly
☐	☒	The statistical test(s) used AND whether they are one- or two-sided *Only common tests should be described solely by name; describe more complex techniques in the Methods section.*
☐	☒	A description of all covariates tested
☐	☒	A description of any assumptions or corrections, such as tests of normality and adjustment for multiple comparisons
☐	☒	A full description of the statistical parameters including central tendency (e.g. means) or other basic estimates (e.g. regression coefficient) AND variation (e.g. standard deviation) or associated estimates of uncertainty (e.g. confidence intervals)
☐	☒	For null hypothesis testing, the test statistic (e.g. *F*, *t*, *r*) with confidence intervals, effect sizes, degrees of freedom and *P* value noted *Give P values as exact values whenever suitable.*
☐	☒	For Bayesian analysis, information on the choice of priors and Markov chain Monte Carlo settings
☐	☒	For hierarchical and complex designs, identification of the appropriate level for tests and full reporting of outcomes
☐	☒	Estimates of effect sizes (e.g. Cohen's *d*, Pearson's *r*), indicating how they were calculated

Our web collection on statistics for biologists contains articles on many of the points above.

Software and code

Policy information about availability of computer code

Data collection	Home-built Labview (version 15.0) software to control microscope
Data analysis	MATLAB (MathWorks, version R2018b), Excel 2016

For manuscripts utilizing custom algorithms or software that are central to the research but not yet described in published literature, software must be made available to editors and reviewers. We strongly encourage code deposition in a community repository (e.g. GitHub). See the Nature Research guidelines for submitting code & software for further information.

Data

Policy information about availability of data

All manuscripts must include a data availability statement. This statement should provide the following information, where applicable:

- Accession codes, unique identifiers, or web links for publicly available datasets
- A list of figures that have associated raw data
- A description of any restrictions on data availability

All data presented in this study are available in the main text and supplementary materials.

Field-specific reporting

Please select the one below that is the best fit for your research. If you are not sure, read the appropriate sections before making your selection.

☒ Life sciences ☐ Behavioural & social sciences ☐ Ecological, evolutionary & environmental sciences

For a reference copy of the document with all sections, see nature.com/documents/nr-reporting-summary-flat.pdf

Life sciences study design

All studies must disclose on these points even when the disclosure is negative.

Sample size	The sample sizes of electrophysiology measurements (number of cells) are around 10, which is common for electrophysiology experiments. These numbers are indicated in tables and figure legends.
Data exclusions	No data exclusion was performed.
Replication	The numbers of replicated experiments are indicated in the main text and figure legends.
Randomization	Labeled cells were chosen in random in imaging experiments.
Blinding	No manual assessment of images was performed.

Reporting for specific materials, systems and methods

We require information from authors about some types of materials, experimental systems and methods used in many studies. Here, indicate whether each material, system or method listed is relevant to your study. If you are not sure if a list item applies to your research, read the appropriate section before selecting a response.

Materials & experimental systems

n/a	Involved in the study
☒	☐ Antibodies
☐	☒ Eukaryotic cell lines
☒	☐ Palaeontology and archaeology
☐	☒ Animals and other organisms
☒	☐ Human research participants
☒	☐ Clinical data
☒	☐ Dual use research of concern

Methods

n/a	Involved in the study
☒	☐ ChIP-seq
☒	☐ Flow cytometry
☒	☐ MRI-based neuroimaging

Eukaryotic cell lines

Policy information about cell lines

Cell line source(s)	Human Embryonic Kidney 293T cells, obtained from Prof. Jing Yang's laboratory at Peking University.
Authentication	Cells have not been authenticated.
Mycoplasma contamination	Cells were not tested for mycoplasma contamination.
Commonly misidentified lines (See ICLAC register)	None.

Animals and other organisms

Policy information about studies involving animals; ARRIVE guidelines recommended for reporting animal research

Laboratory animals	Neonatal rats
Wild animals	The study did not involve wild animals.
Field-collected samples	The study did not involve samples collected from the field.
Ethics oversight	Neonatal rats were purchased from a commercial vendor and no ethical approval or guidance was required.

Note that full information on the approval of the study protocol must also be provided in the manuscript.